THESIS FOR THE DEGREE OF DOCTOR OF PHILOSOPHY

Quantitative chemical imaging to study content release from single nanovesicles

Tho Nguyen

UNIVERSITY OF GOTHENBURG

Department of Chemistry and Molecular Biology

Gothenburg 2023

Thesis for the Degree of Doctor of Philosophy

Quantitative chemical imaging to study content release from single nanovesicles

Tho Nguyen

Duc.khanh.tho.nguyen@gu.se

ISBN 978-91-8069-549-7 (PRINT)
ISBN 978-91-8069-550-3 (PDF)
Available online at http://hdl.handle.net/2077/79036

Department of Chemistry and Molecular Biology
University of Gothenburg
SE-405 30 Göteborg, Sweden

Printed in Borås, Sweden 2023
Printed by Stema Specialtryck AB

Abstract

Cellular communication is vital for the survival of multicellular organisms. This process often relies on a highly regulated mechanism called exocytosis, which involves the release of chemical signals. During exocytosis, vesicles can fully or partially release their contents. The quantity of neurotransmitters expelled in different modes of release may have diverse effects on cellular communication by allowing cells to control the level of outgoing signals. Despite significant discoveries in understanding the components of exocytosis, there is still much to uncover regarding its regulation and implications.

This thesis aims to gain a better understanding of vesicular content release, particularly in the context of partial release, using quantitative chemical imaging. This includes the integration of mass spectrometry imaging (MSI) with electron microscopy or electrochemical analysis alongside light microscopy. By doing so, a comprehensive approach can be employed to gain insights into the mechanism of vesicular content release and quantify the fraction of release. Electrochemical techniques offer the advantage of high temporal resolution and enable quantification of both stored and released molecules from vesicles. Coupled with imaging methods such as fluorescence, electron microscopy, and mass spectrometry imaging, comprehensive spatial information and chemical information can be obtained to complement the data provided by electrochemical techniques. In particular, nanoscale secondary ion mass spectrometry (NanoSIMS), a high-resolution MSI method that is capable of absolute quantification at subcellular level, was primarily used throughout this thesis.

PC12 cells treated with isotopically labeled L-DOPA were examined, and NanoSIMS imaging was correlated with transmission electron microscopy (TEM) to detect and quantify the labeled dopamine in the halo and dense core compartments of large dense core vesicles (LDCVs) in paper I. Paper II introduced a dual-label approach to visualize and quantify vesicles undergoing partial release in PC12 cells by exposing them to a second label during exocytosis. Expanding on the dual-label approach, paper III investigated the influence of vesicle size on the dynamics of partial release. Furthermore, the combination of vesicle impact electrochemical cytometry (VIEC) with live fluorescence imaging was developed in paper IV allowing real-time analysis of vesicular content release from isolated labeled bovine chromaffin vesicles. Overall, these studies demonstrate the application of quantitative chemical imaging in understanding the mechanism and quantifying the fraction of release in vesicular content release.

Sammanfattning på svenska

Cellulär kommunikation är avgörande för överlevnaden hos flercelliga organismer. Denna process är ofta beroende av en noggrant reglerad mekanism som kallas exocytos, vilket innebär frisättning av kemiska signaler. Under exocytos kan vesiklar släppa ut sitt innehåll helt eller partiellt. Mängden neurotransmittorer som drivs ut i olika frisättningssätt kan ha olika effekter på cellulär kommunikation eftersom det kan tillåta cellerna att reglera nivån av utgående signaler. Trots betydande upptäckter om komponenterna i exocytos finns det fortfarande mycket att ta reda på om dess reglering och konsekvenser.

Detta avhandlingsarbete syftar till att få en djupare förståelse för frisättning av vesikulärt innehåll, särskilt i sammanhanget av partiell frisättning, med hjälp av kvantitativ kemisk avbildning. Detta inkluderar integrering av masspektrometriavbildning (MSI) med elektronmikroskopi eller elektrokemisk analys tillsammans med ljusmikroskopi. På så sätt kan en omfattande metod användas för att få insikter i mekanismen för frisättning av vesikulärt innehåll och kvantifiera frisättningsgraden. Elektrokemiska tekniker erbjuder fördelen av hög tidsupplösning och möjliggör kvantifiering av både lagrade och frisatta molekyler från vesiklar. Kombinerat med avbildningsmetoder som fluorescens, elektronmikroskopi och masspektrometriavbildning kan omfattande spatial information och kemisk information erhållas för att komplettera data från elektrokemiska tekniker. I synnerhet användes nanoskalig sekundär jonmasspektrometri (NanoSIMS), en högupplöst MSI-metod som är kapabel till absolut kvantifiering på subcellulär nivå, främst genom hela denna avhandling.

PC12-celler behandlades med isotopmärkt L-DOPA, och NanoSIMS-avbildning korrelerades med transmissionselektronmikroskopi (TEM) för att detektera och kvantifiera det märkta dopaminet inom vesiklar i artikel I. I artikel II introducerades en metod för att visualisera och kvantifiera vesiklar som genomgår partiell frisättning i PC12-celler genom att exponera dem för en andra märkning under exocytos. Genom att bygga vidare på metoden undersökte artikel III inflytandet av vesikelstorlek på dynamiken i partiell frisättning. Dessutom utvecklades kombinationen av vesikelinducerad elektrokemisk cytometri (VIEC) med fluorescensavbildning i realtid med konfokalmikroskopi i artikel IV, vilket möjliggjorde en analys av frisättning av vesikulärt innehåll från isolerade märkta vesiklar. Sammantaget visar dessa studier tillämpningen av kvantitativ kemisk avbildning för att förstå mekanismen och kvantifiera frisättningsgraden vid frisättning av vesikulärt innehål.

List of papers

This thesis is based on the following studies, referred to in the text by their Roman numerals.

I. **Localization and Absolute Quantification of Dopamine in Discrete Intravesicular Compartments Using NanoSIMS Imaging.**

Stefania Rabasco, Tho D. K. Nguyen, Chaoyi Gu, Michael E. Kurczy, Nhu T. N. Phan, and Andrew G. Ewing. *International Journal of Molecular Sciences*. 2022, 23(1), 160.

Participated in designing experiments related to TEM and NanoSIMS. Participated in performing the sample preparation for TEM and NanoSIMS. Participated in data discussion and editing the manuscript with the other authors.

II. **Visualization of Partial Exocytotic Content Release and Chemical Transport into Nanovesicles in Cells.**

Tho D. K. Nguyen, Lisa Mellander, Alicia Lork, Aurélien Thomen, Mai Philipsen, Michael E. Kurczy, Nhu T.N. Phan, and Andrew G. Ewing. *ACS Nano*. 2022. 16 (3), 4831-4842.

Led the project. Designed and performed experiments related to NanoSIMS and single cell amperometry as well as analyzed and interpreted the data. Participated in data discussion. Outlined and wrote the first draft of the paper. Edited the manuscript with the other authors.

III. **Quantitative Nanoscale Secondary Ion Mass Spectrometry (NanoSIMS) Imaging of Individual Vesicles to Investigate the Relation between Fraction of Chemical Release and Vesicle Size.**

Tho D.K. Nguyen[ψ], Stefania Rabasco[ψ], Alicia A. Lork, Andre Du Toit and Andrew G. Ewing. *Angewandte Chemie.* 2023, 62(28), e202304098.

Led the project. Participated in designing and performing experiments related to TEM, NanoSIMS, transfection and confocal imaging. Participated in data analysis and interpretation. Participated in data discussion. Outlined and wrote the first draft of the paper with SR. Edited the manuscript with the other authors.

IV. **Dynamic Visualization and Quantification of Single Vesicle Opening and Content by Coupling Vesicle Impact Electrochemical Cytometry with Confocal Microscopy.**

Ying-Ning Zheng, Tho D. K. Nguyen, Johan Dunevall, Nhu T. N. Phan, and Andrew G. Ewing. *ACS Measurement Science Au.* 2021. 1 (3), 131-138.

Participated in designing and microfabricating the multi electrode array. Participated in designing and performing experiments related to VIEC coupled with confocal imaging. Participated in data analysis. Participated in data discussion and editing the manuscript with the other authors.

[ψ] *These authors contributed equally to the work*

Papers not included in the thesis

Characterization of Stress Granule Protein Turnover in Neuronal Progenitor Cells Using Correlative STED and NanoSIMS Imaging.

Stefania Rabasco, Alicia A. Lork, Emmanuel Berlin, Tho D.K. Nguyen, Nicolas Locker, Carl Ernst, Andrew G. Ewing, and Nhu T.N. Phan. *International Journal of Molecular Sciences.* 2023. 24(3), 2546.

Quantitative Chemical Imaging at the Cellular Level - SIMS, Fluorescence, and Correlative Techniques.

Tho D. K. Nguyen$^{\psi}$, Alicia A, Lork$^{\psi}$, Andrew G. Ewing, Nhu T. N. Phan. In: Single Cell' Omics of Neuronal Cells. Neuromethods, Sweedler, J.V., Eberwine, J., Fraser, S.E. (eds). Humana, New York, NY. 2022. 184, 219-250.

Chemical Analysis of Single Cells and Organelles.

Keke Hu$^{\psi}$, Tho D. K. Nguyen$^{\psi}$, Stefania Rabasco$^{\psi}$, Pieter E. Oomen$^{\psi}$, and Andrew G. Ewing. *Analytical Chemistry.* 2021. 93(1), 41-71.

CONTENTS

Abbreviations

AADC	Aromatic L-amino acid decarboxylase
ADH	Alcohol dehydrogenase
ALDH	Aldehyde dehydrogenase
AR	Aldose reductase
ATP	Adenosine triphosphate
cAMP	Cyclic adenosine monophosphate
CNS	Central nervous system
COMT	Catechol-O-methyl transferase
DA	Dopamine
DBH	Dopamine β-hydroxylase
DESI	Desorption electrospray ionization
DHB	2,5-dihydroxybenzoic acid
DNA	Deoxyribonucleic acid
E	Epinephrine
EGFP	Enhanced green fluorescent protein
FFNs	Fluorescent false neurotransmitters
FIB	Focused ion beam
FT-ICR	Fourier transform ion cyclotron resonance
GA	Glutaraldehyde
HCCA	A-cyano-4-hydroxy-trans-cinnamic acid
IVIEC	Intracellular vesicle impact electrochemical cytometry
LDCVs	Large dense core vesicles
L-DOPA	L-3,4-dihydroxyphenylalanine
m/z	Mass-to-charge ratio
MALDI	Matrix-assisted laser desorption ionization
MAO	Monoamine oxidase
mCLING	Membrane binding fluorophore cysteine lysine palmitoyl group
MEA	Multi-electrode array

MRP	Mass resolving power
MSI	Mass spectrometry imaging
NA	Numerical aperture
NanoSIMS	Nanoscale secondary ion mass spectrometry
NE	Norepinephrine
NPY	Neuropeptide Y
NSF	N-ethylmaleimide-sensitive factor
PC12	Pheochromocytoma 12
PFA	Paraformaldehyde
PNMT	Phenylethanolamine-N-methyl transferase
POI	Protein of interest
ROI	Region of interest
SA	Sinapinic acid
s-AM	S-adenosyl methionine
SCA	Single cell amperometry
SEM	Scanning electron microscopy
SIMS	Secondary ion mass spectrometry
SNAP25	Snaptosome-associated protein 25
SNAREs	Soluble *N*-ethylmaleimide-sensitive factor attachment protein receptors
STED	Stimulated emission depletion microscopy
SVs	Synaptic vesicles
TEM	Transmission electron microscope
TH	Tyrosine hydroxylase
TIRFM	Total internal reflection fluorescence microscopy
TOF	Time-of-flight
UA	Uranyl acetate
v-ATPase	Vacuolar H^+-atpase
VIEC	Vesicle impact electrochemical cytometry
VMATs	Vesicular monoamine transporters
VNUT	Vesicular nucleotide transporter

Chapter 1. Cellular communication

Cellular communication orchestrates the smooth and seamless functioning of multicellular organisms through precise signal transmission. Maintaining effective communication between cells is crucial for normal physiological processes; any dysregulation of this process can result in severe pathologies such as neurodegenerative disorders, autoimmune diseases, or even cancer. Studying the mechanisms underlying cellular communication holds immense importance in addressing these conditions. This chapter aims to provide a basic overview of intercellular and intracellular communication. Moreover, different neurotransmitters will be discussed, with a particular emphasis on catecholamines, an important group of small signaling molecules studied in this thesis.

1.1 Cellular communication

Cellular communication significantly impacts various physiological processes, ranging from immune responses to neuronal firing in the brain. This exchange of information between cells relies on the interplay of chemical and electrical signals, creating a tightly regulated signaling network that ensures appropriate responses to both internal and external stimuli. The release of signaling molecules occurs through a process called exocytosis, which is further described in Chapter 2. Subsequently, these released molecules bind to specific receptors on the surface of other cells, initiating complex intracellular signaling pathways that alter gene expression or metabolic processes.

1.1.1 Intercellular communication

Cell-to-cell communication can occur through various mechanisms, such as paracrine, endocrine, and juxtacrine signaling (examples of the first two are shown in Figure 1). In the juxtacrine mechanism, signaling molecules are passed via direct contact between cells through structures like gap junctions or membrane nanotubes.[1] For instance, in electrical synapses, gap junctions form by multiple connexins hexamer pairing between the membranes of two nerve cells. On the other hand, paracrine signaling is a localized conversation where signaling molecules diffuse through the extracellular matrix to interact with adjacent cell receptors. Paracrine signals evoke rapid responses but are short-lived to maintain communication precision. The concentration of these chemical messengers is often high in the local environment, but enzyme degradation or uptake by neighboring cells facilitates their rapid clearance to prevent unintended effects.[2] Neuronal communication at chemical synapses is a special example of paracrine signaling. In this process, electrical impulses are converted into chemical signals, as neurotransmitters are released into the synaptic cleft, a tiny separation of 50-150 nm between the presynaptic and postsynaptic membranes. The released neurotransmitters act as messengers, carrying essential information between nerve cells. The recipient neuron interprets these biochemical cues, triggering different postsynaptic effects. Depending on the type of neurotransmitter, the postsynaptic neuron is either inhibited or stimulated to continue firing a new electrical impulse along the axon, similar to the relay race of communication.

In our complex body, long-distance communication is also vital. Endocrine signaling is a marathon-like mode of communication that

typically induces a slower response but with a longer-lasting effect. It involves the release of signaling molecules from one part of the body, which then travels through the bloodstream to act on target cells in distant regions. The chemical messengers are produced by specialized endocrine cells in organs such as the thyroid, hypothalamus, pancreas, pituitary, and adrenal glands. Since the signals are "broadcast" over a larger distance, a significant amount of signaling molecules is required during initial secretion to ensure that an adequate concentration of these messengers reaches the target cells. As an example, in response to stress, glucocorticoids produced by adrenal cortex cells (hormonal mechanism),[3] or through direct innervation of adrenal medullary chromaffin cells by the splanchnic nerve (neural mechanism),[4] stimulate the secretion of catecholamines, mostly epinephrine, from the adrenal medulla into circulation (Figure 1). Epinephrine then travels to the heart, for instance, causing a rapid increase in the rate and force of contraction.

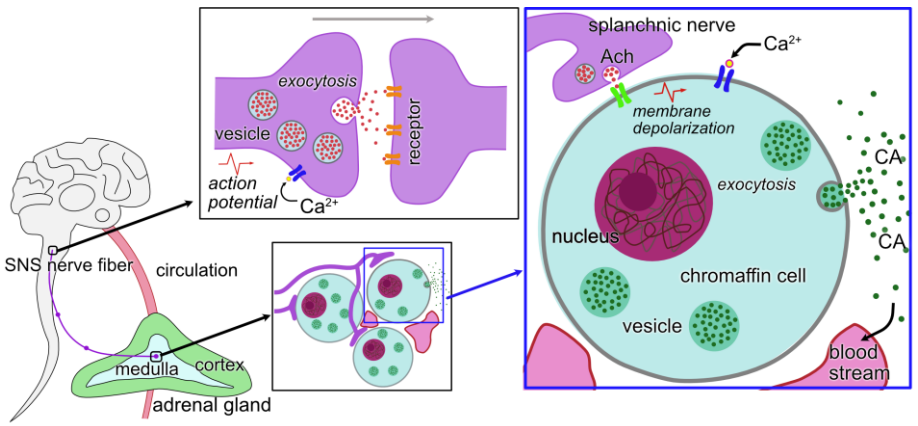

Figure 1. A simplified schematic with examples of paracrine and endocrine mechanisms in cellular communication. Upper gray box: vesicles release neurotransmitters at the synapse, which then diffuse within the synaptic cleft and are taken up by receptors on the receiving neuron. Blue box: sympathetic

neurons release neuroactive molecules acetylcholine, which stimulates chromaffin cells to release catecholamines via exocytosis. Catecholamine molecules then enter the bloodstream and travel to target tissues. SNS: sympathetic nervous system; Ach: acetylcholine; CA: catecholamines. Created based on reference [5].

1.1.2 Intracellular communication

Intracellular communication, on the other hand, refers to the signaling network that operates within individual cells, facilitating the exchange of information between organelles and coordinating various cellular activities. Typically, in the presence of external stimuli, signal transduction by second messenger molecules such as cAMP (cyclic adenosine monophosphate), calcium ions, or phosphorylated proteins initiates an appropriate intracellular response.[6] Many secretory cells, including neurons, endocrine cells, and inflammatory cells, utilize an increase in cytosolic calcium to induce exocytosis.[7,8] For instance, in neurons, synaptic transmission is initiated by fast-moving electrical impulses known as action potentials, which propagate along the axons. An action potential is caused by differences in potassium and sodium levels in the intracellular versus extracellular space due to the synchrony opening of voltage-gated Na^+ and K^+ channels. When this electrical signal reaches the axon terminal, voltage-gated Ca^{2+} channels open, leading to a rapid influx of calcium.[9] As the calcium concentration reaches sufficient levels, it triggers the exocytotic release of neurotransmitters from synaptic vesicles. In endocrine cells like adrenal medullary chromaffin cells, initiation can be caused by a chemical signal. Acetylcholine (Ach) released from preganglionic sympathetic endings at the splanchnic-adrenal synapse binds to nicotinic

acetylcholine receptors and induces sodium influx into chromaffin cells. This causes the depolarization of the cell membrane, triggering the opening of voltage gated Ca^{2+} channels. The increased cytosolic calcium concentration stimulates the transcription of chromogranins and induces the exocytotic release of catecholamines.[10] In many experiments involving pheochromocytoma 12 (PC12) and chromaffin cells, which will be described further in Chapter 3, the exocytotic release was stimulated by a high concentration of potassium solution. When the cells were exposed to high external potassium, the plasma membrane became depolarized, allowing calcium entry through voltage gated Ca^{2+} channels. However, in this case, evoking depolarization by increasing extracellular potassium did not induce an action potential but rather a change in equilibrium potential.[11]

1.2 Neurotransmitters

As previously mentioned, the communication between cells requires the presence of chemical mediators, such as neurotransmitters. By definition, they are chemical substances stocked in synaptic vesicles at the presynaptic neuron, can be released upon depolarization caused by calcium influx, and have specific receptors on the postsynaptic cell membrane.[12] However, this classical description has its limitation, as there are molecules that do not meet all the standards but still serve as neurotransmitters. A prime example is “gasotransmitters” like nitric oxide (NO) and hydrogen sulfide (H_2S), which are produced as needed and not stored in synaptic vesicles or released through exocytosis. Instead, they diffuse from nerve terminals and enter adjacent cells without binding directly to protein receptors.[13,14] Over a hundred

molecules have been identified as neurotransmitters, usually classified into small-molecule and peptide neurotransmitters.[15] Small-molecule transmitters can be further divided into categories such as acetylcholine, amino acids, purines, and biogenic amines (Figure 2). Among the biogenic amines, there is a distinctive subgroup called catecholamines since they all share a hydroxylated benzene ring, catechol moiety. These neurotransmitters are in the focus of this thesis work. Thus, their biological functions, synthesis, deactivation, and metabolic pathways will be introduced in section 1.3.

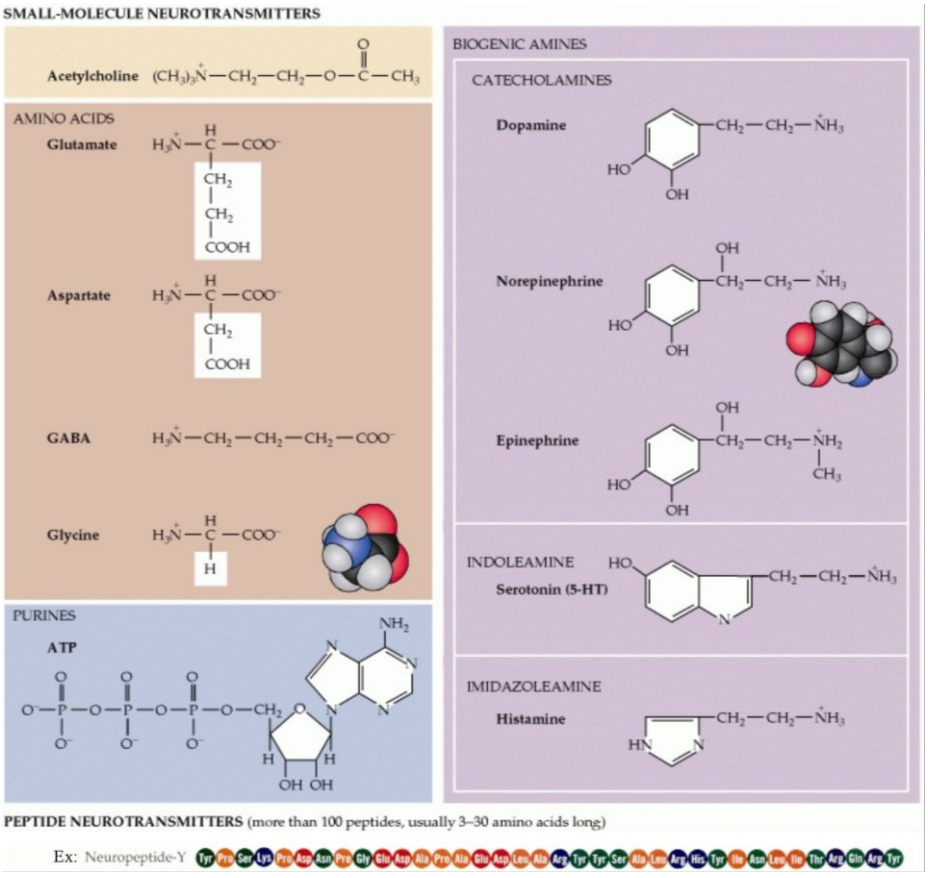

Figure 2. Examples of small-molecule and peptide neurotransmitters. (C: black, H: gray, N: blue, O: red). Adapted with permission from reference [16].

Neurotransmitters play distinct roles in physiological responses due to their chemical and biological functions. Among them, glutamate and aspartate are usually considered excitatory neurotransmitters, while γ-aminobutyric acid (GABA), glycine, and serotonin act as inhibitory neurotransmitters in the matured mammalian central nervous system (CNS).[17] However, it is important to note that certain neurotransmitters (e.g., dopamine, acetylcholine, *etc.*) can exhibit both inhibitory and excitatory effects. This dual functionality depends on the specific receptors present on the postsynaptic (target) cell, as often there are multiple receptors for each neurotransmitter, contributing to this diverse response. Neurotransmitter imbalances can be linked to various diseases and disorders. For example, levels of glutamate and GABA are decreased in individuals with major depressive disorder.[18,19] Deficiencies in biogenic amines, like serotonin, dopamine, norepinephrine, and epinephrine, have also been linked to neuropsychiatric conditions, including bipolar disorder, schizophrenia, and depression.[20–22] Dysfunction in dopamine signaling is also related to addiction, Parkinson's disease, attention-deficit-hyperactivity disorder (ADHD), and Huntington's disease.[23–26]Acetylcholine, an essential transmitter for neuron-to-skeletal muscle cell communication, has been implicated in pathologies like Alzheimer's and Parkinson's diseases.[27,28]

Like the classic neurotransmitters, peptide neurotransmitters are stored in vesicles, transported, and released by exocytosis. Nonetheless, they possess unique characteristics that differentiate them from classic transmitters. For instance, they are synthesized as large precursor molecules and undergo a process where convertase enzymes excise the

desired bioactive peptide(s) from these prepropeptide precursors.[29,30] Once released and reaching their target cells, they almost always act via one or more of a correspondingly G protein-coupled receptors.[31] Peptide neurotransmitters play a critical role in various autonomic responses, nerve development, and regeneration. They are often found together with classical neurotransmitters such as acetylcholine or monoamines. Neuropeptide Y (NPY) is one of the peptide neurotransmitters. NPY is named as such because it contains tyrosine (represented by the single letter amino acid code: Y) at the beginning and end (Figure 2). In mammals, NPY can be found in multiple regions, including the brain, peripheral nerves, adrenal medulla, and vascular endothelium.[32] At the adrenal medulla, it is stored together with catecholamines, chromogranin A and B in chromaffin vesicles. [33–35] NPY has been shown to affect catecholamine release from the adrenal medulla in rats and bovine cells. [36–38] Due to its coexistence in adrenal medullary chromaffin vesicles, NPY can be targeted to label these vesicles for fluorescence imaging while simultaneously measuring catecholamine content using electrochemical techniques. Further details regarding this labeling strategy will be discussed in section 3.2.3.

1.3 Catecholamines

The group of catecholamines consists of dopamine, epinephrine, and norepinephrine. Dopamine (DA) is the precursor for both norepinephrine (NE) and epinephrine (E). It is critical in various activities, including motor and non-motor functions like reward-motivated behavior, addiction, cognition, emotion, and neuroendocrine secretion.[39–41] Dopamine is primarily synthesized and released by the

adrenal medulla. In the brain, dopaminergic neurons are mainly concentrated in the substantia nigra and ventral tegmental areas. Dopaminergic receptors are also present in many other organs, such as the kidneys and heart.[42,43] The dopamine receptor is a type of G-protein coupled receptor. There are five different subtypes of dopamine receptors, namely D1-D5, which can be further classified into two families: D1-like receptors (D1 and D5) or D2-like receptors (D2S, D2L, D3, and D4) due to their basis of pharmacologic properties and the ability to regulate cAMP generation.[44,45] Despite their shared ability to bind dopamine, these two receptor groups differ significantly. In particular, when dopamine binds to D1-like receptors, it triggers the activation of adenylyl cyclase. In contrast, binding to D2-like receptors inhibits adenylyl cyclase and activates potassium channels.

Norepinephrine, or noradrenaline, is the precursor for epinephrine, also called adrenaline. These two neurotransmitters are responsible for regulating heart rate and blood pressure. Particularly, in the presence of stress or danger, their levels can significantly increase to enhance blood flow throughout the body. Like dopamine, they are stored and released from large dense core vesicles in chromaffin cells found in the adrenal medulla. Norepinephrine is also present in nerve cells located in the *locus coeruleus* within the central nervous system and sympathetic nerve terminals. The effects of epinephrine and norepinephrine are mediated by a group of G-protein coupled receptors known as adrenergic receptors. These receptors include α-adrenergic receptors, responsible for smooth muscle contraction and vasoconstriction, and β-adrenergic receptors, responsible for vasodilation, smooth muscle relaxation, bronchodilation, and stimulating cardiac function.[46,47] Adrenergic

stimulation can be stimulatory or inhibitory in cells with appropriate receptors. For example, binding to β receptors (β1, β2, β3) on the postsynaptic membrane increases cAMP levels by activating adenylate cyclase. Binding to α1 receptors increases IP3, resulting in elevated cytosolic calcium levels, while activation of α2 receptors decreases cAMP levels by inhibiting adenylate cyclase.

1.3.1 Catecholamines biosynthetic pathway

The major biosynthetic pathway of catecholamines was first described by Hermann Blaschko back in the 1940s.[48] This pathway initiates with the amino acid tyrosine and progresses through sequential reactions involving four enzymes: tyrosine hydroxylase (TH), aromatic L-amino acid decarboxylase (AADC), dopamine β-hydroxylase (DBH), and phenylethanolamine-N-methyl transferase (PNMT).[49] These enzymes function within different cellular compartments. In the cytosol, TH, AADC, and PMNT drive the conversion of L-tyrosine to L-DOPA, L-DOPA to dopamine, and norepinephrine to epinephrine, respectively (Figure 3A). DBH, localized within the vesicles, facilitates the conversion of dopamine to norepinephrine. For this process to occur, dopamine synthesized in the cytosol must first be transported into the vesicles via vesicular monoamine transporters (VMATs). Subsequently, biosynthesized norepinephrine diffuses out of the vesicle to be converted to epinephrine by PNMT. Finally, epinephrine is packaged back into vesicles by VMATs. In neurons, the expression of these enzymes depends on which catecholamine (e.g., DA, NE, or E) is utilized as a transmitter. In adrenal medulla chromaffin cells, all four of these enzymes are present.[50] However, while the first three enzymes are also expressed in PC12 cells, PNMT is not. Consequently, in PC12 cells,

the primary catecholamine is dopamine, and sometimes small amounts of norepinephrine.

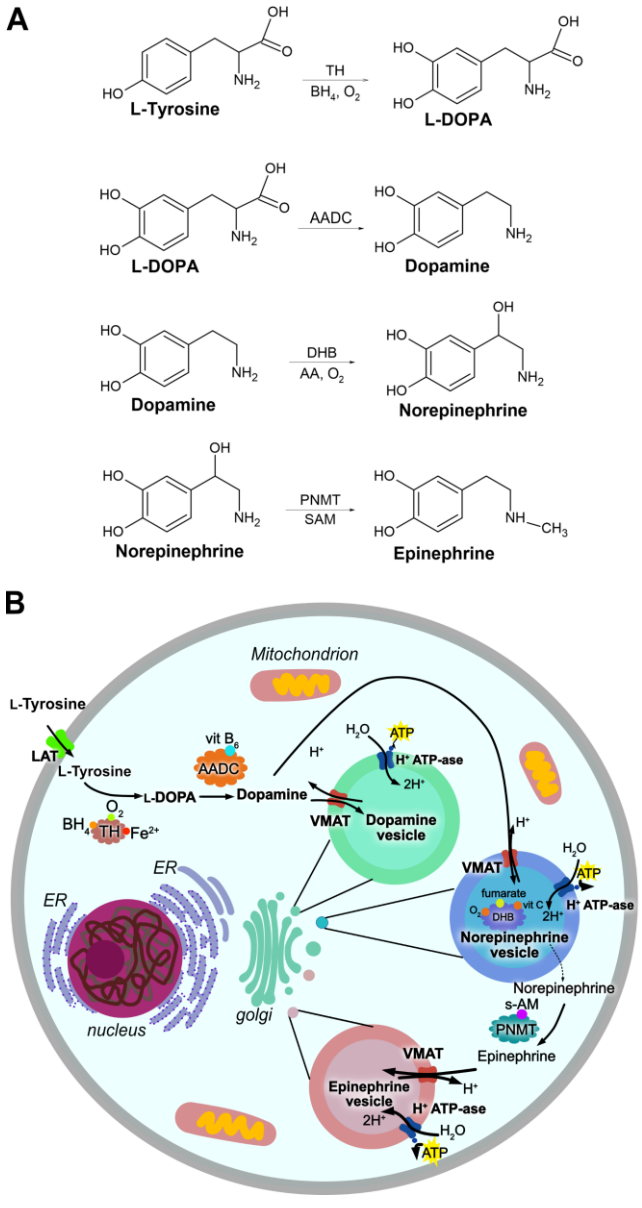

Figure 3. A) Four enzymatic reactions in the catecholamines biosynthetic pathway. B) Schematic of this process in adrenal medulla chromaffin cells. Created based on reference [51].

Figure 3B visually represents this intricate biosynthetic pathway occurring within the adrenal medulla chromaffin cells. To produce L-DOPA from tyrosine, TH uses molecular oxygen (O_2) and biopterin (BH_4) as co-factors to add a hydroxyl group to the meta position of tyrosine. This crucial step is known as the rate-limiting process in the biosynthesis of catecholamines, in which TH utilizes competitive binding between BH_4 and the products (DA, NE, and E) as the inhibitory feedback.[52] In fact, for dopamine synthesis, this rate-limiting behavior of TH can be avoided thanks to the properties of AADC, which possesses a high V_{max} and low K_m for L-DOPA.[53] This allows significant conversion rates from L-DOPA to dopamine by directly increasing the cytosolic L-DOPA levels via L-DOPA incubation, for example.

DBH is a member of a small unique class of copper-containing hydroxylases. This enzyme possesses two copper sites, Cu_H and Cu_M, which are involved in electron transfer; and responsible for binding dioxygen, serving as the site for substrate hydroxylation, respectively.[54] During the reaction, an O atom from molecular O_2 is inserted at the β-carbon in dopamine to form norepinephrine (the second O atom goes to water). The reaction also requires electrons provided a cofactor, ascorbic acid (Vitamin C).[55]

By transferring a methyl group from S-adenosyl methionine (s-AM) to the nitrogen of norepinephrine, PNMT catalyzes the conversion of norepinephrine to epinephrine, a secondary amine. The expression of PNMT in chromaffin cells is controlled by glucocorticoid hormones released from the nearby cortical cells.[56]

1.3.2 Catecholamine metabolic pathway

The reuptake and metabolism of catecholamines play a significant role in regulating their levels and terminating neurotransmission. The metabolic pathway of catecholamines is facilitated by several enzymes, including the major enzymes monoamine oxidase (MAO) and catechol-O-methyl transferase (COMT), along with others like aldose reductase (AR), alcohol dehydrogenase (ADH), and aldehyde dehydrogenase (ALDH) found in different parts of the body (Figure 4).

MAO is located on the outer membrane of mitochondria in various cell types, working to remove the amine group.[57] In the brain, MAO is primarily found in nerve terminals and glia, while in the periphery, it is mainly present in the liver and kidney. MAO has two isoforms, MAO-A, mainly present in dopaminergic and noradrenergic neurons, and MAO-B, the primary form in serotonergic neurons and glia.[58] On the other hand, COMT is present in the cytosol and works by adding a methyl group to the 3 OH position of the catechol ring. COMT also has two isoforms: membrane-bound (MB-COMT), predominantly expressed in brain neurons, and soluble (S-COMT) in other tissues such as the liver, blood, and kidney.[59,60] MAO participates in regulating the cytoplasmic DA that has passively leaked from vesicular storage. In contrast, DA released through exocytosis for signal transduction ends its signaling by being reimported to the presynaptic neuron, recycled or uptaken by surrounding cells, and degraded by COMT, MAO, AR, ADH, and ALDH. In the brain, the main degradation products of DA are DOPAC in rats and HVA in primates, while in the periphery, that is HVA. The metabolic pathway of norepinephrine is similar to that of dopamine. The primary end product of norepinephrine metabolism in

the brain is MHPG; in the periphery, it is vanillomandelic acid (VMA). VMA is formed in the liver from circulating MHPG through a two-step process involving the intermediate MOPEGAL and enzymes ADH and ALDH.[61]

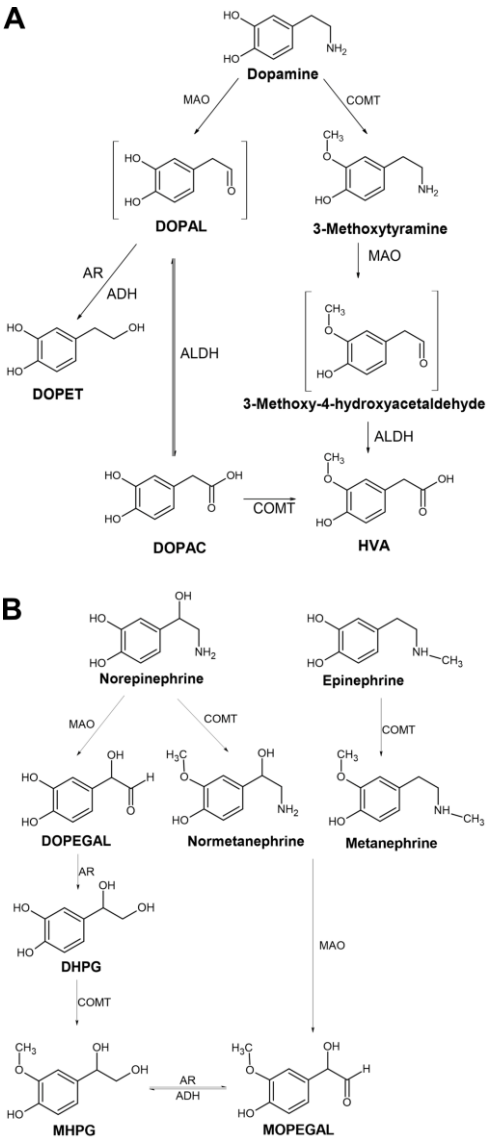

Figure 4. Deactivation and metabolic pathways of A) dopamine, B) norepinephrine and epinephrine.

Chapter 2. Exocytosis

Secretory vesicles facilitate intercellular communication by releasing transmitter molecules into the extracellular space through a process called exocytosis. These vesicles contain chemical messengers and a complex system of proteins, lipids, and other molecules that tightly regulate exocytosis. This chapter aims to provide an introductory understanding of exocytosis, including the structure and components of vesicles, their biogenesis, and the machinery and mechanisms involved. Additionally, the chapter will discuss the three modes of vesicular content release, with a particular focus on partial release as the main mechanism explored in this thesis. Furthermore, the chapter will also introduce commonly used cellular models for studying exocytosis.

2.1 Vesicles

Vesicles, or granules, are small spherical organelles enclosed by a membrane. These secretory organelles can be categorized into synaptic vesicles (SVs) and large dense core vesicles (LDCVs), distinguished by their size and composition. SVs commonly found in the CNS are typically small, measuring around 50 nm in diameter.[62–64] When stained observed under a transmission electron microscope (TEM), SVs appear relatively clear. On the other hand, LDCVs are present not only in the CNS but also in other tissues, for instance, pancreatic beta cells and especially adrenal chromaffin cells.[65–67] They are significantly larger, with a diameter reaching up to 350 nm. In TEM images, LDCVs display an electron-dense core easily distinguishable from its surrounding halo

as the proteins being stained by osmium tetroxide/ uranyl acetate (see section 3.3.2).

The biogenesis pathway of LDCVs in neuroendocrine cells is still largely unknown. However, the process is believed to involve several steps, starting with synthesizing the dense core protein matrix.[68,69] These components are packaged in the trans-Golgi network along with recruited membrane proteins. Following this, loaded LDCVs bud off and undergo further maturation while continuing to be loaded with catecholamines, then moving toward the plasma membrane for later release. Membrane proteins can also be recycled after exocytosis.[70] This understanding has come from studies conducted in different models such as PC12 cells, bovine and mouse chromaffin cells.[71–73]

The dense core within LDCVs comprises various soluble acidic proteins, predominantly chromogranins (Cgs) like CgA and CgB, as well as secretogranin II (SgII).[69] Additionally, LDCVs contain bioactive peptides like NPY and enkephalins.[74,75] Modulating the protein content of the dense core can impact the storage and release of neurotransmitters.[36–38,76] The attraction between the negatively charged amino acid residues in the dense core proteins and the protonated catecholamines within the acidic intravesicular environment is thought to contribute to their association.[77] Localization and quantification of labeled dopamine within the dense core and halo of LDCVs showed the preferential storage of dopamine in the dense core (**paper I**).[78] Vesicles also serve as reservoirs for ions like Ca^{2+}, H^{+}, as well as adenosine triphosphate (ATP). Overall, the composition includes approximately 0.5 to 1 M of catecholamines, around 120 to 200 mM ATP, roughly 40

mM bound Ca^{2+} (chelated with other intravesicular components), and about 50 μM free Ca^{2+}.[79–81] The ability of vesicles to hold such high concentrations of solutes while maintaining osmotic pressure is facilitated by the association of solutes and dense core components.[82–85] It is worth noting that ATP and Ca^{2+} are essential elements for vesicle transport and exocytosis, thus it is likely not a coincidence that they store high levels of these substances, but rather a deliberate design to support these processes.[86,87]

The membrane of the vesicle is a phospholipid bilayer decorated with various proteins serving distinct functions. There are transporter proteins responsible for loading the vesicular contents, such as vacuolar H^+-ATPase (v-ATPase), vesicular monoamine transporters (VMATs), and vesicular nucleotide transporter (VNUT). V-ATPase is a proton pump working to acidify the vesicles. The v-ATPase consists of two domains operating through a rotational mechanism. ATP hydrolysis occurs in the V_1 domain, leading to movement within a central rotary complex that ultimately transports protons across the integral V_0 domain.[88] As a result, the pH inside the vesicle drops to approximately 5.5, in contrast to the pH of approximately 7.4 found in the cytosol and extracellular space. This pH gradient regulates the formation of dense core granules by controlling the aggregation ability of CgA.[89] VMATs use the pH difference and the membrane potential (positive inside) to actively transport neurotransmitters into the vesicle.[90] In this process, two protons are pumped out in exchange for one cationic catecholamine molecule. This mechanism is illustrated in Figure 3B. VNUT, on the other hand, accumulates ATP into the vesicle, pumping in one ATP molecule for each expelled proton and operating in a membrane

potential-dependent manner.[91] Besides the transporters, vesicle membranes are also associated with a protein machinery (e.g., the SNAREs) that facilitates the process of calcium-dependent exocytosis. Their respective functions in each step of exocytosis will be described in section 2.2.

The accurate movement of vesicles during their lifecycle significantly depends on the essential interplay between motor proteins and cytoskeletal filaments. Motor proteins like kinesins, dyneins, and myosins, recognize and bind to specific adaptor proteins on the vesicle membrane, enabling accurate transport and delivery to specific cellular locations. These molecular motor proteins comprise large protein families with diverse functions.[92] Despite employing different mechanisms, they all exploit the energy from ATP hydrolysis to produce the force required for transporting cargo-filled vesicles.[93] For effective vesicle movement, microtubules and actin filaments serve as tracks for motor proteins within the cytoplasm. The polarity of these tracks determines the directionality of transport. Kinesins and dyneins move along microtubules, whereas myosin motors operate on actin filaments. Notably, the actin network is most concentrated near the plasma membrane, including sites of vesicle release. These motor proteins and filaments have also been shown to contribute to the recruitment of vesicles to the release sites involved in Ca^{2+}-regulated exocytosis.[94–97] The role of actin in regulating the fusion process, particularly the stability of the fusion pore, has also been suggested.[98]

2.2 Exocytosis

Following their biogenesis, vesicles are transported to the release site. Upon receiving signals for exocytosis (as discussed earlier in section 1.1.2), intracellular signaling pathways coordinate the recruitment and interaction of functional components, preparing the vesicles for the exocytosis process. Exocytosis entails the docking, priming, and fusion of vesicles with the plasma membrane and later the release of their contents. However, the exact definition and necessity of these steps for functional release remain debated.

The minimal exocytotic machinery typically includes soluble N-ethylmaleimide-sensitive (NSF) factor attachment protein receptors (SNAREs), synaptotagmins, complexins, and munc18.[99] The SNAREs consist of synaptobrevin, syntaxin, and synaptosome-associated protein 25 (SNAP25). Depending on their locations on the vesicle or target membrane, these proteins can be classified as v-SNARE or t-SNARE. Specifically, synaptobrevin is associated with the vesicle membrane, while syntaxin and SNAP25 are associated with the plasma membrane. These proteins interact zipper-like to overcome repulsive forces and pull the two membranes closer together to facilitate vesicle fusion. Figure 5 illustrates the steps involved in exocytosis and the corresponding proteins.

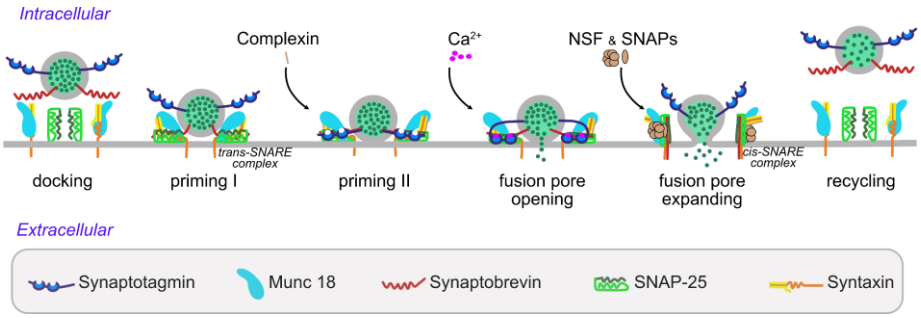

Figure 5. A schematic representation of some critical steps during exocytosis to release neurotransmitters and vesicle recycling after exocytosis. During priming, synaptobrevin (v-SNARE), syntaxin-1, and SNAP-25 (t-SNARE) assemble into a *trans*-SNARE complex. Complexin further enhances this complex. Calcium triggers fusion pore opening by binding to synaptotagmin, facilitating interaction of synaptotagmin with SNAREs and phospholipids. The expanding fusion pore transforms the *trans*-SNARE complex into *cis*-SNARE complexes, which are eventually dissociated by NSF/SNAP ATPases for vesicle recycling. Create based on reference [100].

In general, docking refers to the recruitment and retention of vesicles at the active site near the plasma membrane.[101] Priming, on the other hand, is an ATP-dependent process that renders the vesicles release-ready.[101,102] Kinetically, priming is considered the most advanced step as the v-SNAREs and t-SNAREs have already formed partially zippered trans-SNARE complexes, a stable four-helix bundle.[103,104] The interaction between munc18 and syntaxin has been proposed to facilitate the formation of the SNARE complex.[103,105] Additionally, complexin acts as a grappling protein, enhancing the stability of zippered SNARE complexes and placing them in an activated but immobilized state. This state is released upon calcium ions entering and binding to synaptotagmin.[106,107]

Synaptotagmin is thought to induce a positive curvature in the vesicle membrane when calcium binds. This curvature effectively lowers the activation energy barrier required for the fusion of the vesicle membrane with the plasma membrane, thereby facilitating SNARE-mediated fusion.[108] This process ultimately creates a fusion pore, enabling the release of the vesicle contents into the extracellular space. Furthermore, it has been proposed that synaptotagmin not only plays a crucial role in calcium-triggered membrane fusion but also contributes to the expansion of the fusion pore.[109] Also, dynamin and actin have been proposed with evidence supporting their involvement in the opening and closing phases of the fusion pore.[96,110,111] Besides, the role of lipids in the vesicle fusion process should not be underestimated. The membranes where the SNARE proteins reside consist of various phospholipid species, sphingolipids, and cholesterol. To facilitate fusion, the lipid structure of both membranes needs to be reorganized, and extra lipids might be necessary to expand the fusion pore. Several phospholipids have been found to participate in regulating exocytosis and influence the dynamics of the fusion pore.[112–114] Moreover, polyunsaturated fatty acids has also been proposed to act on syntaxin, promoting the formation of the SNARE complex, which directly participates in vesicle fusion.[115]

Once fusion has occurred, the SNAREs are in the low-energy cis-SNARE complex. The α-soluble N-ethylmaleimide-sensitive factor attachment protein (α-SNAP) and NSF sequentially bind to the SNARE complex, forming a 20S complex. Within this complex, NSF utilizes the energy obtained from ATP hydrolysis to disassemble the SNARE complex, effectively recycling its subunits.[116] The recycled vesicles can again be loaded with transmitters for the next round of exocytosis.

2.3 Different modes of exocytotic release

Exocytosis is a highly complex and tightly regulated process. While we have made significant discoveries regarding its critical components, there is still much that remains unknown about the regulation of exocytosis and its implications. During exocytosis, it has been shown that the vesicle may undergo full release where it fuses completely with the plasma membrane, resulting in the release of all its contents (known as all-or-none or full release),[117,118] or it can release only a portion of its contents before closing again. Fractional release can occur through two mechanisms: kiss-and-run and partial release. Kiss-and-run is a mode of exocytosis where a flickering fusion pore allows for the release of a small amount of neurotransmitter before quickly resealing.[119–123] On the other hand, partial release, sometimes referred to as open and closed, sub-quantal release, or selective secretion, involves a larger fusion pore allowing for the escape of a more substantial fraction of the neurotransmitter.[111,124–129] While the term “kiss and run” primarily describes the process, “partial release” emphasizes the crucial aspect of the amount of transmitter being released. These different modes of release have a significant impact on the quantity of transmitter being released. Consequently, they may initiate various responses in cellular communication by allowing cells to regulate the level of outgoing signals. Figure 6 provides a representation of these three release modes.

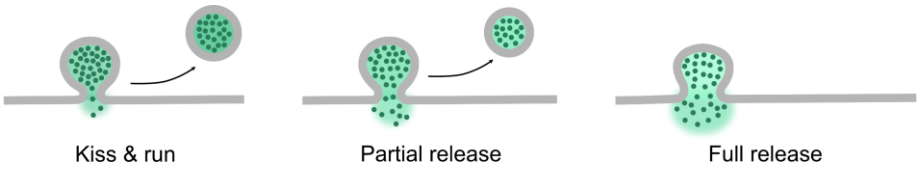

Figure 6. A scheme illustrates various modes of exocytosis, namely kiss-and-run, partial release, and full release. It also demonstrates the variations observed in the fraction of transmitters being released among these modes.

Partial release, in many ways, has been suggested to be an important mode of fusion. This mechanism not only facilitates rapid and efficient vesicle recycling but also plays a crucial role in regulating and controlling the rate of transmitter secretion. Additionally, it could potentially provide the necessary machinery for adjusting synaptic strength and achieving synaptic plasticity, which are thought to be vital for cognitive processes, learning, and addressing certain diseases. Despite a growing amount of supporting literature, whether partial release is a predominant mechanism is still subject to scientific debate. Recent advancements in methodology have enabled measuring and comparing both the amount of released transmitters and the total content within vesicles.[79,130–133] Numerous studies have demonstrated that the total content of a secretory vesicle is larger than the amount released during exocytosis. In other words, only a fraction of the cargo within a secretory vesicle is released. For example, research conducted on different cell types and organisms has revealed different fractions of transmitter release. In pheochromocytoma (PC12) cells, up to 60% of the cargo is released during a typical exocytotic event.[130] Repetitive stimulation in PC12 cells has resulted in release ranges from approximately 60% to 80%.[134] Similarly, adrenal chromaffin cells release around 50% of the cargo, and this percentage increases to 85%

after high ATP concentration incubation.[135] Human carcinoid BON cells release approximately 80% of the cargo, while pancreatic beta-cells release roughly 30%.[136,137] In living Drosophila larval neuromuscular neurons, the release is only around 10%.[127] The measurement of the fraction of released transmitters serves as a crucial parameter, offering quantitative insights into the extent of partial release and aiding in the understanding of whether a specific fraction is associated with certain characteristics of the vesicles (**paper II**).[138]

Previous studies have also provided evidence that, after exocytotic events, a majority of vesicles undergo rapid endocytosis (independent of clathrin). Interestingly, the rate of endocytosis overlaps significantly with the rate of exocytosis.[139] These results suggest a tight coordination between the processes of vesicle release and retrieval. Furthermore, research has shown that synaptic vesicles proteins are capable of undergoing recycling multiple times, potentially up to a few hundred cycles over a span of approximately 24 hours.[140] These findings support the idea that vesicles can undergo multiple partial release rather than complete depletion. Additionally, mathematical models have highlighted the relatively small required opening angle of the fusion pore for neurotransmitter release, implying that a complete opening of the fusion pore may not be necessary for neurotransmitter release.[141] Direct visualization of fusion pore closure through advanced microscopy techniques for example total internal reflection fluorescence microscopy (TIRFM) and super-resolution stimulated emission depletion microscopy (STED) has further supported the concept of partial release.[111,125,142] In addition, the visualization and quantification of vesicle contents during partial release using mass spectrometry

imaging (MSI) techniques like nanoscale secondary ion mass spectrometry (NanoSIMS) have also contributed to this understanding (**paper II**).[143]

The extent of partial release is believed to be influenced by the intracellular calcium concentration, which can be modulated by the strength of stimuli or specific pharmaceuticals. Normally, calcium functions as a secondary messenger, which can activate protein kinase C, resulting in the phosphorylation of proteins like munc18 or myosin light chain kinase, both crucial in the exocytosis process.[144–146] Studies have shown that as intracellular calcium levels increase due to stronger stimuli, there is a significant rise in the amount of neurotransmitters released. This effect was observed by increasing the frequency of stimuli while maintaining a fixed extracellular calcium concentration or by altering the extracellular calcium concentration while keeping a fixed stimulation frequency.[147] Similar observations were made when comparing low-frequency stimulation with 10 mM K^+ stimulation and high-frequency stimulation with 30 mM K^+.[148] Furthermore, elevated intracellular calcium levels has also shown to promote the rearrangement of filamentous actin, leading to an increase in the frequency of exocytosis release events and the amount of molecules released per event.[96]

2.4 Cellular models

Different simplified biological models are available for studying cellular communication, particularly regulated secretion, exocytosis. These models range from cell-derived systems to animal models and serve as valuable tools to investigate the intricate details of exocytosis and the

underlying molecular mechanisms. For instance, chromaffin cells derived from the adrenal medulla are extensively used to study neurotransmitter release, and pancreatic beta cells for investigating insulin secretion. Besides, animal models such as rats, mice, zebrafish, or fruit fly (e.g., *Drosophila melanogaster*), are also widely used, providing a more holistic view of exocytosis in a complex physiological context. The selection of appropriate biological models depends on the specific scientific question at hand. In this thesis, PC12 cells and chromaffin cells (Figure 7) are the cell models employed, and this section will discuss their background and relevance in studying vesicular content release.

2.4.1 Chromaffin cells

Albert von Kölliker was the first to describe the adrenal medulla, the innermost part of the adrenal gland, highlighting its distinct structure and function in comparison to the cortex. This discovery was made through a histochemical reaction using chromate salts.[69] This reaction primarily occurred in the adrenal medulla due to a reduction by epinephrine in the presence of chromium.[149] Consequently, these cells were named "chromaffin cells" to signify this phenomenon.

Chromaffin cells consist of adrenergic cells, which mostly produce epinephrine, and noradrenergic cells, which mainly produce norepinephrine.[150] It is possible to isolate these cells from the adrenal glands and grow them in primary cultures, which can be sustained for a few days. Exocytotic release in chromaffin cells can be stimulated by a high concentration of potassium or barium solutions.[151] Although the exact mechanisms by which barium initiates exocytosis are still unclear,

some proposed theories have emerged. One theory suggests that barium compete with calcium within the exocytotic machinery, while another theory posits that barium can trigger the release of calcium from its intracellular stores.[152,153] The vesicle components, biogenesis, and exocytotic machinery have been mentioned earlier in sections 2.1 and 2.2. Figure 7 displays the typical morphology and structure of isolated bovine chromaffin cells.

A chromaffin cell contains a large amount of LDCVs, accounting for almost 30% of its total volume.[67] These vesicles can also be isolated from the chromaffin cells via centrifugation of the homogenates of the adrenal medulla and used as a "model" organelle.[154–156] The average diameter of chromaffin LDCVs is about 300 nm, and they can hold up to about 0.5 M to 0.9 M of catecholamine.[67,157] The large size and high catecholamine content enhance the visibility of these vesicles in imaging methods and improve the detection of individual vesicle release events when using electrochemical techniques. However, due to their limited lifespan and inability to regenerate through propagation, additional effort is required in creating new cultures for each experiment preparation.

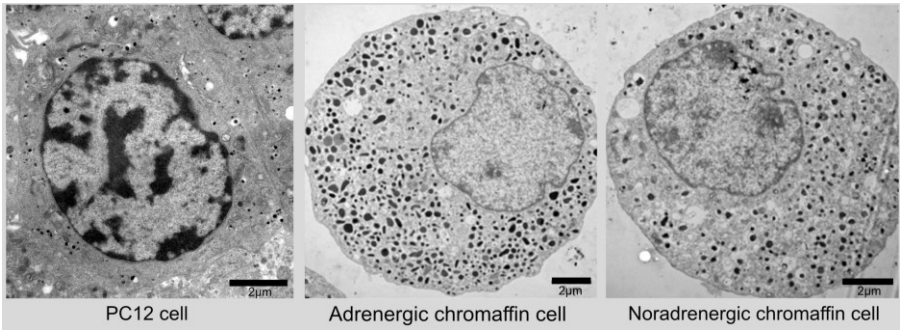

Figure 7. TEM images of a PC12 cell and chromaffin cells. The images of chromaffin cells were reprinted with permission from reference [158].

2.4.2 PC12 cells

PC12 cells are a widely used immortal cell line in the field of neural differentiation and neurosecretion research.[159] They were first isolated from a pheochromocytoma (a neuroendocrine tumor) found in rat adrenal medulla. This significant finding was made in 1976 by Lloyd Greene and his colleagues.[160] PC12 cells are highly suitable for laboratory cultures and have been extensively studied, resulting in a wealth of knowledge about their growth and differentiation. When exposed to nerve growth factor, PC12 cells undergo differentiation and exhibit characteristics similar to sympathetic ganglion neurons, including the development of neuron-like processes and varicosities.[161] As a result, PC12 cells serve as a compelling model for investigating exocytosis in both neuronal and endocrine systems. When PC12 cells are in an undifferentiated state, they typically exhibit a round shape (Figure 7). PC12 cells also contain LDCVs, similar to those described in chromaffin cells. The size of PC12 vesicles varies between 50-200 nm, and they can store approximately 0.1 M of catecholamines, mainly dopamine, along with minor amounts of norepinephrine.[162] In terms of pharmacological manipulation, by exposing PC12 cells to substances like L-DOPA (a dopamine precursor) (also used in **paper I, II, III**) or reserpine (a VMAT inhibitor), their vesicle volume and catecholamine accumulation can be modulated.[130,163] In experimental settings, exposing PC12 cells to a high concentration of potassium solution is a commonly used method to induce exocytosis, as it directly depolarizes the membrane and rapidly triggers the process.[164]

Overall, PC12 cells have several advantages compared to primary neurons or chromaffin cells, as they offer better consistency across

batches and are relatively easy to produce. However, it is important to consider certain drawbacks associated with PC12 cells to ensure the reliability and quality of data. One disadvantage is that being a cancer cell line, PC12 cells can undergo genetic changes over multiple passages, leading to the development of sub-clones within the cell line. It is often advisable to monitor the number of passages during the culturing process and to consider it when comparing data.

Chapter 3. Methods

The quantity and distribution of neurotransmitters, proteins, and other regulatory factors are of great interest in gaining a deeper understanding of exocytosis. Exploring different modes of release may help us comprehend why and how they impact the level of outgoing signals in cellular communication. This chapter aims to provide an overview of imaging and electrochemical techniques utilized in this field. It covers mass spectrometry imaging, microscopy, and amperometry, highlighting relevant applications and recent advancements. The primary focus is on mass spectrometry imaging of neurotransmitters, specifically emphasizing nanoscale secondary ion mass spectrometry (NanoSIMS), which allows high-resolution imaging and quantification of dopamine. The methodology for integrating mass spectrometry imaging with electron microscopy and electrochemical analysis with fluorescence microscopy will also be described, along with the strengths and weaknesses of each technique.

3.1 Mass spectrometry imaging

3.1.1 Overview of mass spectrometry imaging

Mass spectrometry imaging (MSI) encompasses a range of techniques that enable the mapping of various molecules, providing insights into the spatial and molecular complexity of biological samples. In MSI, a desorption and ionization probe, such as a laser or ion beam, is used to scan a sample surface pixel-by-pixel. At each measurement position, molecules are desorbed and ionized, subsequently collected and analyzed by a mass analyzer that separates ions based on their mass-to-

charge ratio (m/z). A mass spectrum representing the abundance of different molecules as a function of their m/z is generated at each measurement coordinate. By compiling this collection of mass spectra, specific ion images can be reconstructed, visualizing the abundance of each m/z value across the sample area (Figure 8).

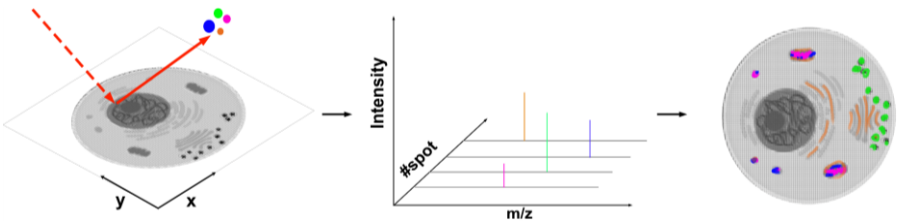

Figure 8. Schematic illustrating the process of mass spectrometry imaging. MSI involves using an ionization probe to scan the surface of a sample. At every position (x_i, y_i) of the surface, a mass spectrum is produced. By combining these spectra, an image is generated. This allows visualization of the distribution of specific ions.

The most common MSI methods for imaging biological samples include secondary ion mass spectrometry (SIMS), matrix-assisted laser desorption ionization (MALDI), and desorption electrospray ionization (DESI). These techniques are distinctive due to their different ionization mechanisms. They also provide varying selectivity and sensitivity to different classes of analytes and differences in throughput and spatial resolution. Figure 9 summarizes the characteristics of these techniques.

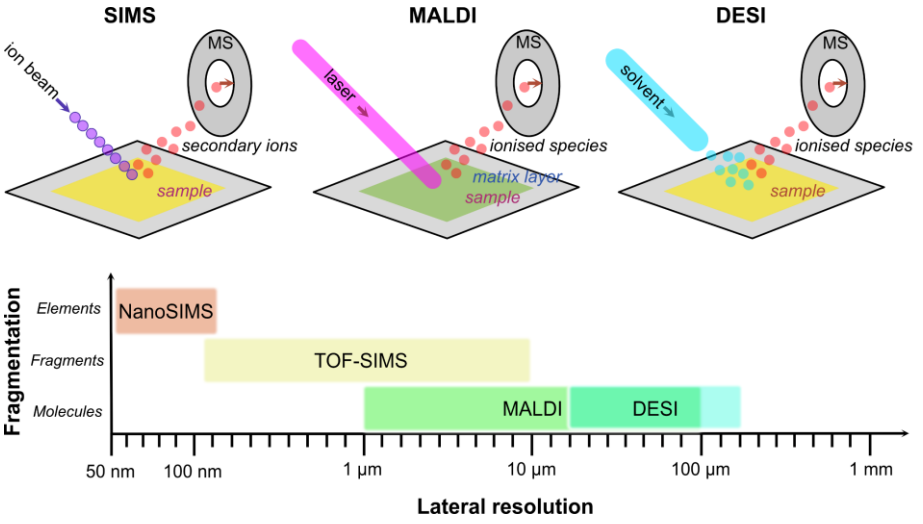

Figure 9. An overview of different MSI techniques, including their lateral resolution and the level of fragmentation. SIMS techniques, such as NanoSIMS and TOF-SIMS, employ a primary ion beam to desorb ions from the sample surface. MALDI is a softer ionization technique utilizing a laser to irradiate the sample, with the assistance of UV-absorbing matrix. DESI involves directing a spray of ionized solvent toward the sample surface for desorption. Unlike MALDI and SIMS, DESI is performed at ambient conditions, resulting in different analytical capabilities. SIMS techniques offer excellent spatial resolution but typically result in fragmentation in the mass spectrum. DESI offers relatively lower spatial resolution in comparison, but is associated with minimal fragmentation. Created based on the references [165,166].

Secondary ion mass spectrometry (SIMS). In the early 1960s, the initial application of mass spectrometry to chemical imaging was marked by the development of an imaging SIMS instrument by Raymond Castaing and George Slodzian, as well as the creation of the first scanning ion microprobe by Helmut Liebl and Richard Herzog.[167–169] SIMS involves using a primary ion beam to bombard and sputter the

surface of a solid sample, generating secondary ions that can be extracted and analyzed by a mass spectrometer. These secondary ions provide valuable information on the elemental, molecular, isotopic compositional, and spatial organization at the surface or within samples, depending on the mode of operation (static or dynamic). Static SIMS, introduced around 1969 by Alfred Benninghoven, uses a low intensity primary ion beam to remove only the very top surface layer and generates larger mass fragments, allowing the acquisition of molecular information.[170] Static SIMS is considered a valuable soft ionization technique for surface analysis. Nowadays, time-of-flight instruments (TOF-SIMS) are standard instruments for static SIMS, although variations exist. On the other hand, dynamic SIMS uses a focused high-energy primary ion beam, exceeding the static limit of 10^{13} ions/cm^2, which leads to higher secondary ion production, increased sensitivity, but also more fragmentation, causing a loss of molecular information as only atomic or diatomic ions can be detected. Dynamic SIMS is particularly useful in the semiconductor industry for identifying trace chemical components and characterizing device structures due to its excellent depth profiling capabilities. In the past several decades, SIMS has undergone significant advancements in primary ion sources, including the promotion of secondary ion generation using oxygen (for an increase in positive ion emission), cesium (for an increase in negative ion emission), noble metals, as well as molecular and cluster primary ions.[171–174] Additionally, efforts have been made to improve instrumental aspects such as parallel mass registration and high transmission. Overall, SIMS offers several advantages for surface analysis and mass spectrometry imaging, including surface sensitivity, high mass resolution, and imaging capability down to microscopic levels with

flexible ion sources and easy focusing of ion beams in ultrahigh vacuum conditions. The latest generation of dynamic SIMS instruments, referred to as nanoscale secondary ion mass spectrometry (NanoSIMS), has revolutionized molecular imaging by achieving a lateral resolution of 50 nm.[175] Recently, cryoNanoSIMS has also been developed.[176] In section 3.1.3, more details regarding NanoSIMS will be provided. Additionally, there is the IOG 25Ga, a focused ion beam (FIB) system that utilizes a liquid metal ion source to generate a highly focused ion beam capable of achieving a spot size as small as 50 nm.[177] These advancements have paved the way for significant progress in mass spectrometry imaging from the tissue level to the organelle scale, opening up new possibilities in the field.[178,179]

Matrix-assisted laser desorption ionization (MALDI). In MALDI, a laser is utilized to irradiate a sample that is placed on a conductive plate together with a matrix. The matrix, typically an organic molecule, absorbs the laser energy and converts it into electronically excited energy, transforming the solid mixture of the matrix and analyte into a gaseous state, facilitating desorption/ionization (Figure 9). MALDI is recognized as a soft ionization technique, causing minimal fragmentation, and primarily generating molecular ions. It provides high throughput and sensitivity for detecting large, nonvolatile, and thermally labile compounds such as proteins, lipids, peptides, and polymers. Common matrices used in MALDI include 2,5-dihydroxybenzoic acid (DHB), α-cyano-4-hydroxy-trans-cinnamic acid (HCCA), and sinapinic acid (SA), among others. In the 1990s, Bernhard Spengler and Richard Caprioli pioneered the use of MALDI for mass spectrometry imaging.[180,181] In terms of spatial resolution, MALDI-MSI typically

achieves roughly 50 μm, but with optimal settings, it can reach 1 to 5 μm.[166] Despite the improvement, this lateral resolution still restricts its practical use for imaging at the single cell level. Traditionally, MALDI has been coupled with a time-of-flight (TOF) mass analyzer due to its fast acquisition speed and unlimited mass range.[182] However, recent advancements have introduced alternative mass analyzers, such as Fourier transform ion cyclotron resonance (FT-ICR) or orbitrap, which offer improved mass resolution and accuracy.[183,184] One challenge with conventional matrices used in MALDI is the high background signals that can interfere with detection of low molecular weight compounds and peptides in the low mass range. Recent developments have focused on utilizing novel high ionization efficiency matrices, implementing new matrix deposition procedures, and employing in situ sample treatments, such as on-tissue chemical derivatization.[185–188]

Desorption electrospray ionization (DESI). DESI is an ambient ionization technique that was developed based on the concept of electrospray ionization and was first introduced in the 2000s.[189] In DESI, charged droplets of solvent are directed onto the sample surface, producing secondary charged droplets containing the desorbed analytes. When these droplets rapidly evaporate, the surface area decreases without reducing the surface charge. This leads to a coulombic explosion, efficiently ejecting molecular ions. By using different spraying solutions, DESI allows selective ionization of molecules of interest. DESI offers significant advantages for in vivo analysis of various analytes, ranging from small molecules to lipids and proteins, as it operates under ambient conditions and requires almost no sample preparation. However, the spatial resolution of DESI-MSI is primarily

constrained by the size of the droplet spray and the efficiency of secondary ion transfer to the mass spectrometer, among other key parameters. Typically, the spatial resolution of DESI-MSI ranges from approximately 40 to 200 μm, thereby limiting its application mainly to tissue imaging.[190] Nonetheless, recent advancements have focused on improving the lateral resolution and sensitivity of the technique. One significant advancement in DESI is the introduction of nanospray desorption electrospray ionization (nanoDESI). This technique utilizes finer capillaries and shorter distances between them, resulting in an improved spatial resolution of approximately 10 μm.[191]

Overall, in single-cell mass spectrometry analysis, MALDI and SIMS are the two main commonly used ionization techniques.[192] SIMS offers exceptional lateral resolution when it comes to cellular imaging. In contrast, MALDI has emerged as the preferred method for analyzing large intact biomolecules but often utilizing chemical fingerprinting over imaging.

3.1.2 MSI of small-molecule neurotransmitters

MSI is now widely recognized as an effective tool for studying brain tissues in neurological diseases such as Parkinson's and Alzheimer's disease, among others. However, the focus has primarily been on analyzing lipids, peptides, and proteins, with many fewer studies done on small-molecule neurotransmitters despite their importance in the functioning of the nervous system.[193–197] This is due to several challenges, such as their low molecular weight (typically less than 200 Da), poor ionization efficiency, very low concentrations in vivo, and background interference signals from matrices or other tissue

components in the lower mass range.[198] To address these challenges, new instrumentation designs incorporating high resolution mass analyzers, such as the orbitrap, have been introduced.[199] The use of suitable chemical derivatization agents that improve limits of detection and specifically target neurotransmitters and their metabolites has also become highly useful.[187] Several on-tissue derivatization strategies, focusing on either the primary amine or catechol functional groups, have allowed the detection of monoamine neurotransmitters using MALDI.[200,201] However, in some cases, the use of additional matrices after derivatization is still necessary. For neurotransmitters that are prone to postmortem degradation, like acetylcholine, very well-controlled sample preparation has been developed to minimize the effect.[202,203] Furthermore, the application of NanoSIMS imaging to detect isotopically labeled monoamine neurotransmitters has proven to be an extremely effective approach.[78,138,143,204,205] Table 1 summarizes typical examples of MSI methods that have been used to analyze monoamine neurotransmitters, ranging from tissue level to subcellular scale.

Table 1. Examples of MSI methods for detecting and analyzing monoamine neurotransmitters

Target molecules	Lateral resolution level	Sample preparation/ Matrices	MSI method	Ref.
Monoamine neurotransmitter: Dopamine Epinephrine Norepinephrine Serotonin	Tissue	-	DESI	206
		TPP	DESI	207
		-	IR-MALDESI	208,209
		CA	MALDI	210
		FMP-10	MALDI	198
		Zinc oxide nanoparticles	MALDI	211
		mTRAQ derivatization	MALDI	212
		DPP derivatization with DHB matrix	MALDI	213
		TAHS, CA, and DPP-TFB derivatization, with DHB matrix	MALDI	187
		4-(N-Methyl) pyridinium boronic acid derivatization	TOF-SIMS LDI-TOF	201
	Single cell	-	3D OrbiSIMS	199
	Organelle	Resin embedded, TEM	NanoSIMS	78,138,143, 204,205

TPP: 2,4,6-triphenylpyrylium tetrafluoroborate. CA: 4-hydroxy-3-methoxycinnamaldehyde. FMP-10: 4- (anthracen-9-yl)-2-fluoro-1-methylpyridin-1-ium iodide. mTRAQ: mass differential tags for relative and absolute quantification. DPP: 2,4-diphenyl-pyranylium. TAHS: *p*-*N*,*N*,*N*-trimethylammonioanilyl *N*-hydroxysuccinimidyl carbamate iodide. DPP-TFB: 2,3-diphenyl-pyranylium tetrafluoro-borate. DHB: 2,5-Dihydroxybenozic acid. TEM: transmission electron microscopy. IR-MALDESI: infrared matrix-assisted laser desorption electrospray ionization. LDI: laser desorption/ionization. SIMS: secondary ion mass spectrometry. TOF: time of flight.

3.1.3 NanoSIMS imaging

NanoSIMS is a dynamic SIMS technique known for its high spatial resolution, but also destructive nature towards the sample. The high-energy primary ion bombardment intentionally breaks all molecular bonds, resulting in the generation of monoatomic and diatomic secondary ions. Therefore, molecules of interest must either possess specific elements for detection or be isotopically labeled. NanoSIMS offers exceptional capabilities in elemental analysis and isotopic identification again thanks to its high mass resolution and excellent lateral resolution. This enables the spatial localization of rare isotope enrichment on the sample surface. Ongoing efforts are expanding NanoSIMS applications in various areas of life sciences such as biology, neuroscience, as well as pharmacology. For example, it has been employed to investigate the dynamics of stable isotope uptake and metabolism in biological specimens by measuring isotopic ratios.[214–217] Several NanoSIMS-detectable probes to label specific proteins via click chemistry or immunostaining have been developed, opening up more possibilities for cellular imaging.[218,219] Furthermore, NanoSIMS has also been utilized to reveal the distribution of different pharmaceuticals in cells.[220–223]

The NanoSIMS instrument usually comes with two switchable reactive primary ion sources: Cs^+ for analyzing electronegative secondary ions and O^-/O^{2+} for analyzing electropositive secondary ions.[224] For the work included in this thesis (**papers I, II, III**), the Cs^+ primary ion source was used. A simplified schematic of the NanoSIMS and examples of ion images are shown in Figure 10.

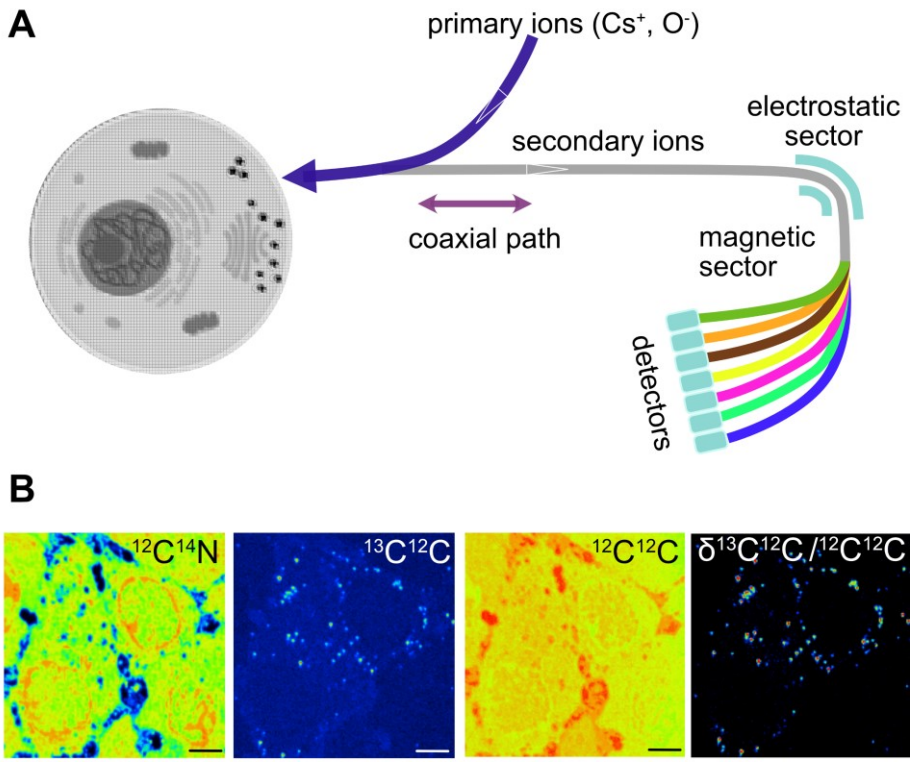

Figure 10. (A) Simplified schematic of NanoSIMS instrument. The surface of the sample is scanned using a focused high-energy primary ion beam. Secondary ions are then extracted and analyzed by a dual-focusing sector mass analyzer. It is possible to detect up to seven ions simultaneously from each measurement position. (B) Examples of secondary ion ($^{12}C^{14}N^-$, $^{13}C^{12}C^-$ and $^{12}C_2^-$) images and $^{13}C^{12}C^-/^{12}C_2^-$ ratio image of PC12 cells treated with ^{13}C L DOPA acquired with NanoSIMS.

A signature feature of the NanoSIMS instrument is its co-axial column that allows the objective lens of the primary ion column and extraction optics to be placed much closer to the sample. This configuration offers the highest beam density (i.e., the highest beam current in the smallest spot size) and ensures a maximized and uniform collection of the

secondary ions. As a result, the cesium primary ion beam can, under ideal conditions, achieve a lateral resolution of 25-50 nm.[225] Also, a new RF plasma O^- primary ion source with higher brightness has been introduced to replace the duoplasmatron source, which can provide a beam with a diameter of 40 nm, comparable to the performance of the cesium source.[225]

Generally, the final resolution of an image is often affected by various factors including sample properties (e.g., density, topography) and instrumental parameters such as the primary ion beam, D1 aperture, pixel resolution, and sputtering dwell-time. One way to improve the lateral resolution is by using a smaller primary ion beam and higher pixel resolution to mitigate the beam mixing effect, allowing clearer distinction of adjacent features. A fundamental challenge that arises with the improvement of lateral resolution is that the sensitivity tends to decrease due to the reduced amount of material available to be sputtered and ionized. Oversampling can be employed, wherein a small primary beam but larger than the pixel size is used, enabling certain parts of the sample surface to be probed more than once, resulting in an increased secondary ion yield and ultimately improved resolution. Overall, it is not only important to effectively collect the secondary ions but also to ensure their efficient transmission. The NanoSIMS instrument encompasses a focusing system that utilizes lenses, deviating plates, and apertures to shape the beam, minimize aberrations, and optimize transmission. This ensures that as many secondary ions as possible enter the mass spectrometer. Figure 11 shows a detailed schematic of the Cameca NanoSIMS 50L.

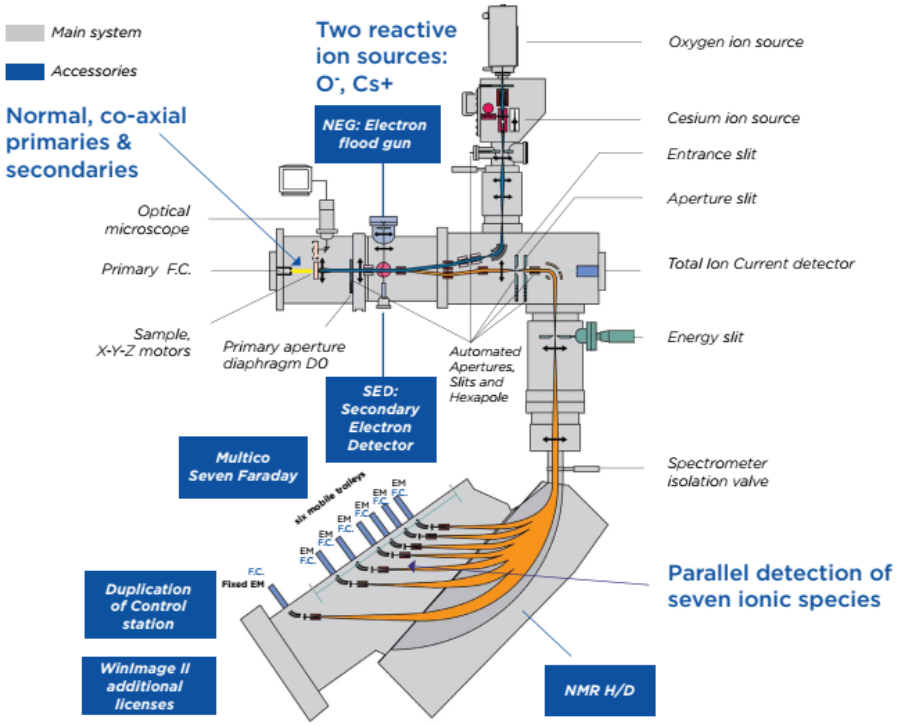

Figure 11. A detailed schematic of the Cameca NanoSIMS 50L. This schematic illustrates the co-axial configuration of the primary and secondary ion beam, along with a series of ion lenses and slits that extract and guide the secondary ions to an electrostatic sector and then to the magnetic sector for separation based on their m/z. For detection, the instrument is equipped with one EM (Electron Multiplier) and one FC (Faraday Cup) on each trolley. FCs are essential for achieving high precision isotope ratios with reproducibility at the low tenth per mil level across the entire scanned area. However, FCs do not provide fast imaging capabilities like EMs do. Reproduced with permission from reference [225].

The extracted secondary ions are separated based on their m/z using a dual-focusing sector mass analyzer. This separation process involves an electrostatic filter followed by a magnetic sector. The electrostatic sector

separates the secondary ions based on their kinetic energy regardless of their m/z. Later, an energy slit at the exit of this sector allows the selection of ions within a specific energy range. Then, in the magnetic sector, a magnetic field is used to deflect the ions, curving their path based on their m/z. Consequently, the combination allows ions with the same m/z ratio but different initial kinetic energy to be concentrated at a focal point, ultimately resulting in improved transmission of sputtered ions (up to 40 %). Additionally, the dual-focusing sector mass analyzer provides high mass resolution (up to 10000), enough to resolve isobaric interferences. The Cameca NanoSIMS 50L allows multicollection of seven selectable ionic species (electron multiplier/ Faraday cup detectors) in parallel. Electron multipliers are commonly used for imaging mode due to faster response time compared to Faraday cups. Intensity maps are then generated to depict the distribution and relative abundance of the selected ions in each pixel of the image.

Mass resolution refers to the ability to distinguish between secondary ions that have different m/z, defined as M/dM, where M represents the mass of the ion of interest and dM is the difference in mass between the ion of interest and its adjacent ion. Mass resolution and mass resolving power (MRP) are terms that are often used interchangeably, but they refer to distinct properties that define different aspects of performance in analytical methods and instruments. MRP is specifically associated with instrument-related performance.[226] In the case of the Cameca NanoSIMS 50L, the MRP is inversely proportional to the magnification of the spectrometer and the width of the entrance slit. Since magnification is directly related to the radius, the MRP remains theoretically constant along the focal plane. However, angular and

chromatic aberrations can degrade the theoretical mass resolution. Mass resolution thus can be taken as M/dM = R/4 * L10-90, where R represents the trajectory radius and L10-90 corresponds to the line width that encompasses 80 % of the intensity.[225]

Lateral resolution, also called spatial resolution, describes the minimum distance needed to resolve objects in an image. In SIMS imaging, it is defined as the ability of the instrument to separate signals from two adjacent locations and is usually determined by extracting the 16%-84% intensity line-scan from the image (e.g., across edge of sample feature).[225]

Relative abundance measurement (δ) is often expressed in per mille (‰, parts per thousand) as:

$$\delta^X \text{‰} = \frac{{}^X R_{sample}}{{}^X R_{reference}} \times 1000 - 1000 \quad (1)$$

Here X is ^{13}C, ^{15}N, ^{2}H, ^{18}O, ^{34}S..., R_{sample} is the isotopic ratio of the sample, and $R_{reference}$ is the isotopic ratio of the reference, for instance, $^{13}C_{VPDB} = {}^{13}C/{}^{12}C = 0.0112372$, $^{15}N_{air} = {}^{15}N/{}^{14}N = 0.0003676$, $^{2}H_{VSMOW} = {}^{2}H/{}^{1}H = 0.00015576$, $^{18}O_{VSMOW} = {}^{18}O/{}^{16}O = 0.0020052$, $^{34}S_{VCDT} = {}^{34}S/{}^{32}S = 0.045005$ (VSMOW: Vienna Standard Mean Ocean Water; VPDB: Vienna Pee Dee Belemnite; VCDT: Vienna Canyon Diablo Troilite).[227,228]

3.1.4 Quantitative NanoSIMS imaging of ^{13}C dopamine

The intensities of secondary ion signals and isotopic ratios obtained in NanoSIMS measurements can also be converted into concentrations.

However, in order to achieve accurate results, it is important to make appropriate corrections for any ion suppression and matrix effects. Additionally, the use of carefully constructed standards is recommended. The standard should be a sample with a known concentration of the element of interest and should have the same chemical composition matrix as the sample being studied.[229] Nevertheless, when it comes to biological samples, reproducing such a complex matrix material within the cellular environment can be quite challenging. For NanoSIMS analysis of cell samples, a common method involves preparing resin-embedded samples similar to TEM specimens. In this preparation technique, almost all the intracellular water content is replaced by epoxy resin. This allows using a spiked resin, which contains a stable-labeled version of the analyte or a similar compound, as a calibration standard for absolute quantification.[222]

Regarding the study of vesicle content release using quantitative NanoSIMS, the use of ^{13}C labeled neurotransmitters has been employed. This labeling approach enables the tracking of the fate of vesicles before and after release events as well as distribution of the labeled neurotransmitter within vesicular compartments.[78,138,204] In these studies, PC12 cells are typically incubated with ^{13}C L-DOPA, which is converted to ^{13}C dopamine by the enzyme AADC and actively loaded into vesicles by VMATs (see section 1.3.1) resulting in a high enrichment of ^{13}C inside the vesicles (Figure 12). Recently, Thomen et al. presented an approach to directly determine the absolute concentration in resin-embedded cells from the $^{13}C/^{12}C$ ratio, taking into account contributions from the biomass, the epoxy resin infiltrated in the cell, and the ^{13}C dopamine detected at the region of interest (ROI).[205] Through elemental

analysis and ion yield measurements, they demonstrated that the epoxy resin (Agar100) and resin-embedded cell contained uniformly distributed carbon content (54 M) and the matrix effects. This allows a straightforward conversion of ^{13}C enrichments (from ^{13}C-labeled dopamine) (equation 2) into concentrations, using the carbon background as a standard (equation 3).

$$\delta^{13}C\ ‰ = \frac{{}^{13}C^{-} / {}^{12}C^{-}}{{}^{13}C_{VPDB}} \times 1000 - 1000 \quad (2)$$

$$\left[{}^{13}C\ dopamine\right](M) = \frac{\left(\delta^{13}C_{ROI} - \delta^{13}C_{control}\right)}{1000} \times \frac{{}^{13}C_{VPDB} \times 54M}{N^{13}C} \quad (3)$$

Here, $\delta^{13}C_{ROI}$ is the ^{13}C enrichment from ROIs of the treated sample and $\delta^{13}C_{control}$ is the enrichment in a blank resin calculated relative to the reference material $^{13}C_{VPDB}$ = 0.0112372, in per mille (‰). $N^{13}C$ corresponds to the number of labels incorporated in the molecule of interest. In this case N = 6.

The images and quantitative information obtained from NanoSIMS are more valuable when considered within a biological context. Hence, electron microscopy techniques like TEM and scanning electron microscopy (SEM) are often used to complement the NanoSIMS data. These techniques provide detailed morphological information and enable the identification of subcellular structures. In this regard, correlative TEM-NanoSIMS, has been employed in the studies presented in **papers I, II, and III**. This approach offers a new method for measuring the release fraction of transmitters and provides both visual and quantitative insights into the extent of partial release. Further details regarding TEM will be discussed in the subsequent sections.

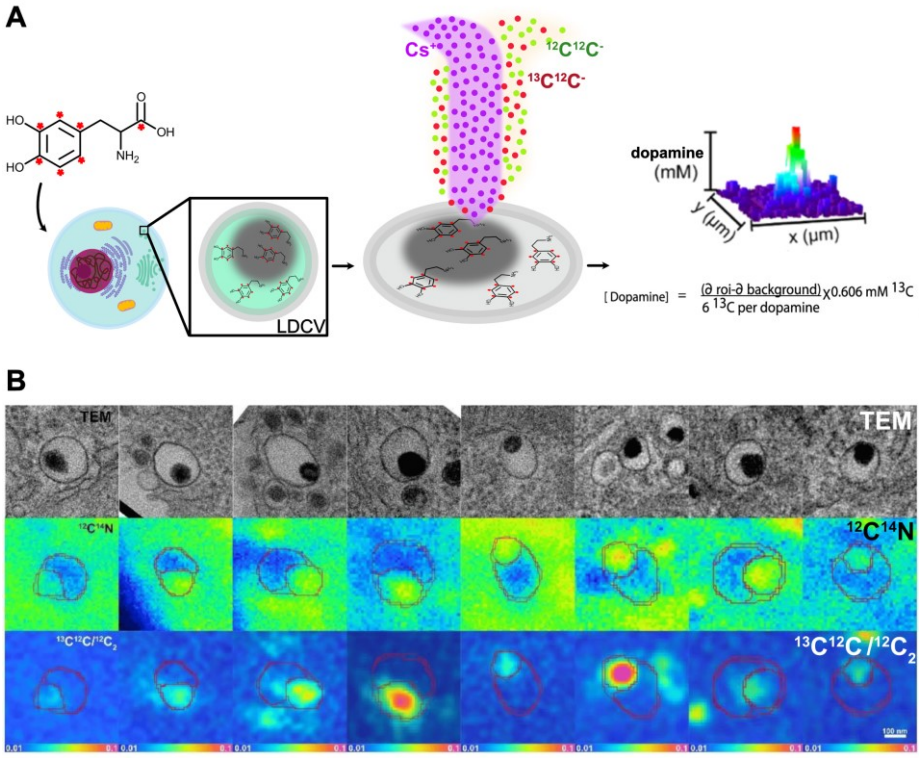

Figure 12. (A) Schematic illustrating the strategy to label the LDCVs with ^{13}C L-DOPA for quantitative NanoSIMS analysis. This approach enables the conversion of measured ^{13}C enrichments into absolute concentrations of ^{13}C-labeled dopamine within individual secretory vesicles in PC12 cells. The rightmost panel is adapted with permission from reference [33]. (B) Images demonstrating the compartmentalization between the dense core and halo in eight different LDCVs from PC12 cells that were embedded in resin and sectioned. Top: TEM images of the vesicles showing the halo and dense core compartments. Middle: $^{12}C^{14}N^-$ secondary ion images of the vesicles obtained from NanoSIMS. Bottom: $^{13}C^{12}C^-/^{12}C_2^-$ HSI images. The scale bar is 100 nm. Adapted with permission from reference [78].

3.2 Microscopy

Different microscopy techniques use specific mediums such as electrons or photons that interact with a sample to generate an image of it. Since these techniques are based on different principles, they require different instrumentations and sample preparations, ultimately offering a diverse range of resolutions.

Lateral resolution refers to the ability to distinguish individual points from each other. In microscopy, it is determined by the minimum distance at which points can be separated as individual entities. This can be calculated using the Rayleigh-based formula: $r = (0.61\lambda)/NA$, where r represents the resolution, λ is the wavelength of light (or emission wavelength in fluorescence microscopy), and NA is the numerical aperture. The numerical aperture of an objective lens determines its resolving power. However, the total resolution of the microscope optical system also depends on the numerical aperture of the substage condenser; a higher numerical aperture leads to better resolution. In other words, when the numerical aperture is fixed, the choice of wavelength used to observe the object influences the resolution. Thus, conventional optical microscopy using visible light (400-700 nm) offers a maximum resolution of approximately 200 nm. On the other hand, electrons can have much shorter wavelengths especially when accelerated to high speeds.[230] For instance, with an accelerating voltage of 120 keV, the electron wavelength reduces to approximately 0.004 nm, enabling a theoretical resolution of around 0.2 nm in TEM images.

3.2.1 Electron microscopy

Ernst Ruska proposed the idea of electron microscopy in 1928, and developed the first practical transmission electron microscope in the 1930s in collaboration with Max Knoll.[231] In 1986, Ruska was awarded the Nobel Prize in Physics for the work in electron optics and designing the first electron microscope.[232]

Transmission electron microscopy (TEM) uses a high voltage electron beam to visualize specimens with a significantly higher resolution compared to fluorescence microscopy. In a TEM instrument, electrons are emitted from an electron gun located at the top of the microscope's vacuum tube. These electrons are then focused into a fine beam using electromagnetic lenses along the tube. As the electron beam passes through the sample, it either scatters or hits a screen at the bottom of the microscope, creating an image. This image reveals different compartments of the specimen in various shades based on their density. The main components of a TEM instrument, along with some example TEM images, are shown in Figure 13. One limitation of TEM is that electrons can only be transmitted through very thin specimens. Therefore, in the case of biological samples like cells or tissues, several steps, including fixation, dehydration, resin embedding, and ultrathin sectioning, are often necessary to prepare the samples for TEM analysis. However, it should be noted that extensive sample preparation such as staining proteins and/or lipids with heavy metals can negatively impact the final image resolution. These stains can create a uniform appearance, making it more challenging to resolve the ultrastructural features. Moreover, improper sample preparation causing heavy metal precipitation can also introduce artifacts, further compromising the

image quality. Additionally, very thin samples are more susceptible to deformation, tearing, and damage from the high-energy electron beam used in imaging. Overall, the resolution of TEM images for biological samples depends on multiple factors. However, TEM remains an excellent tool for visualizing and resolving subcellular features at the nanometer scale. This capability is particularly crucial for visualization and size measurements of LDCVs within the context of this thesis.

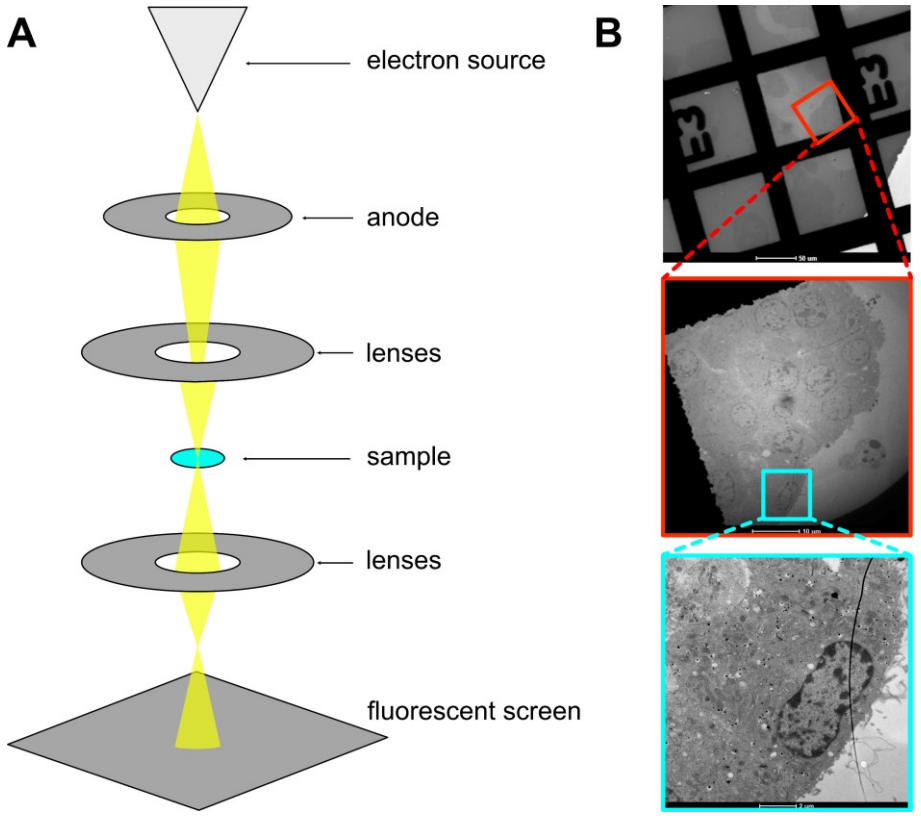

Figure 13. A simplified schematic illustrating the principle of a TEM instrument with the main components (A), A finder grid as seen in the TEM with the "zoom-in" TEM image of a cluster of cells and finally an image of a single PC12 cell (B).

The development of another technique called cryo-electron microscopy (cryo-EM), which involves rapidly freezing samples to cryogenic temperatures to fix them, instead of using chemicals, has expanded the possibilities in the field, particularly in structural biology.[233,234] Cryo-EM is widely employed for studying protein structures and is now capable of obtaining the high-resolution structures of proteins with very low molecular weights, such as a 52 kDa protein resolved at 3.2 Å.[235] Nonetheless, the technique still experiences limitations in terms of throughput due to the extensive optimization requirements and the time-consuming nature of data collection and processing.

Scanning electron microscope (SEM) is a technique closely related to TEM and was first introduced in the 1940s.[236] SEM uses a focused beam of high-energy electrons to scan across the surface of a conductive specimen, causing the emission of secondary electrons. The scattered electrons are then collected and counted, ultimately generating an image. The signal intensity at each pixel depends on the number of secondary electrons detected. In the backscattered electron mode, the microscope detects the high-energy electrons that are produced by the elastic scattering of the primary beam electrons with the atom nuclei. The production of backscattered electrons varies based on the weight of the element being scanned. Generally, heavier elements, due to their larger nuclei, are able to deflect the incident electrons more strongly than lighter elements. This difference in deflection results in a more pronounced contrast, making heavier elements appear brighter in the image. This technique is valuable for providing information regarding the samples' surface topography and some chemical compositions.

3.2.2 Correlative TEM - NanoSIMS

In the field of life sciences, the ability to obtain high-resolution chemical maps of nanoscale sub-cellular structures is of immense value for understanding the underlying mechanisms behind various physiological processes, diseases, and therapeutics. However, there is a fundamental limit between resolution and sensitivity that cannot be surpassed. This limitation arises from the finite number of atoms that can be accommodated within a given voxel size. To illustrate, if a voxel has the capacity to hold 10^3 atoms, the lowest theoretically detectable and localizable dopant concentration within this voxel would be $1/10^3$ or 0.1 at % (Figure 14).[237]

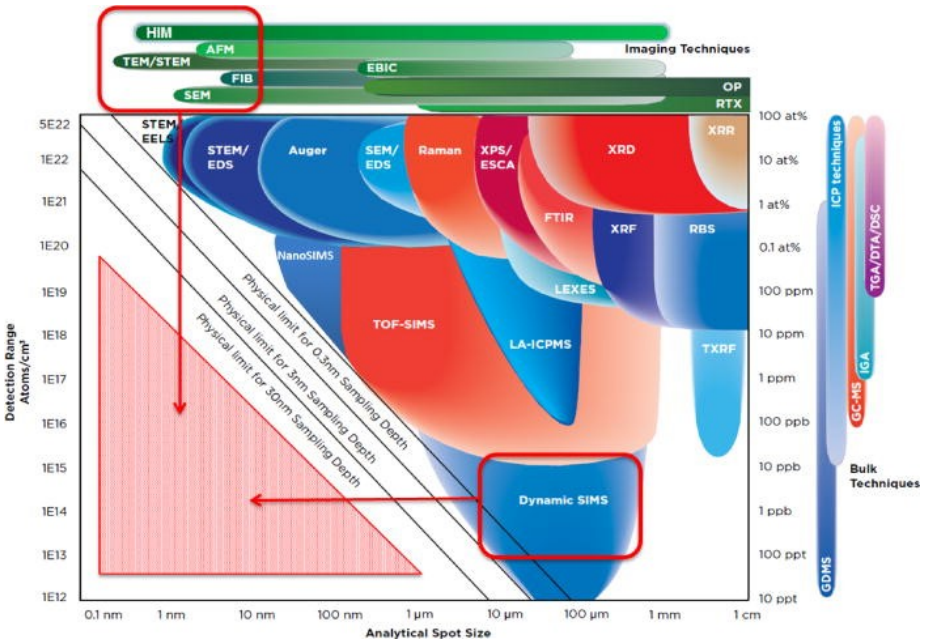

Figure 14. The lateral resolution-sensitivity comparison of different analytical techniques. Reproduced with permission from reference [237].

In Figure 14, a visual summary demonstrates the different analytical techniques and their positions in the resolution-sensitivity landscape. The combination of electron microscopy and NanoSIMS imaging emerges as a powerful and complementary approach. This innovative paradigm allows the correlation of high-sensitivity and relatively high-resolution chemical images from NanoSIMS with ultra-high-resolution structural images from EM. Moreover, these images are obtained from the exact same ROI, providing a comprehensive and integrated understanding of the studied sub-cellular structures.

Biological sample preparation for correlative TEM - NanoSIMS

NanoSIMS imaging requires samples that are compatible with ultra-high vacuum conditions, have limited topography, and are conductive to minimize sample charging during the analysis. To prepare biological samples for NanoSIMS, the most common method is adopted from the techniques used in TEM. This typically includes steps such as chemical fixation, contrasting, dehydration, resin embedding, and sectioning.

Chemical fixation is crucial for preserving the structure and stability of the components within the sample. Glutaraldehyde (GA) and paraformaldehyde (PFA) are commonly used in primary fixation to stabilize the ultrastructure before further processing. These aldehydes penetrate into the biological material and cross-link proteins and DNA bases.[238] GA can also react with phospholipids containing free amino groups (e.g., phosphatidylethanolamine, phosphatidylserine).[239] GA penetrates slower than PFA, making it more suitable for thin samples like cell monolayers, while a mixture of GA and PFA is preferred for thicker samples like tissues.[240] In the secondary fixation step, osmium

tetroxide (OsO_4) is often used to cross-link lipids, particularly unsaturated fatty acid chains of phospholipids, as well as certain lipoprotein complexes. This ensures that the membranes are fixed and prevents their extraction during dehydration. Careful washing of the samples with suitable buffers, including the addition of primary amide like glycine, helps remove excess aldehydes to avoid precipitates and non-specific binding during subsequent steps such as antibody labeling. Uranyl acetate (UA) can be added to improve contrast in TEM images, allowing better discernment of ultrastructure within the sample. However, it should be noted that UA can precipitate at pH ~7.4 and in the presence of salts, so filtering the solution and carrying out the staining step in the dark is necessary. Additional washing steps with water help remove salts or residue from fixation.

After fixation and contrasting, the samples are dehydrated using ethanol or acetone solutions. Here the water content of the sample is replaced with the alcohol, starting at low concentration, and gradually increasing to minimize shrinking effects. The specimens are then infiltrated and embedded with resin, typically epoxy resin. This involves replacing the solvent with gradually increasing concentrations of liquid resin and cured with heat or UV light to form a hard block. Once embedded, the sample can be sectioned for imaging. In NanoSIMS, a thicker section compared to TEM (~70 nm) is required to obtain a steady state sputtering rate and prevent sample breakage during the measurement. For absolute quantitative analysis, samples of around 300 nm thickness are desired since achieving the steady state sputtering rate requires a certain amount of Cs^+ ions to be implanted into the sample surface,

resulting in a loss of material (up to approximately 180 nm depth) during the reactive implantation.[205]

When preparing sample sections for correlative TEM and NanoSIMS analysis, it is important to place them on a substrate that is compatible with both instruments, such as EM copper grids. For accurate identification of the exact position of a cell during both TEM and NanoSIMS analysis, using finder grids is highly recommended. These finder grids contain reference points that are visible in both systems. Due to the destructive nature of NanoSIMS on samples, it is common practice to perform TEM imaging before conducting NanoSIMS analysis. Once the TEM imaging is completed, the sample can then be subjected to NanoSIMS. To avoid charging during NanoSIMS measurements, the sample sections are often coated with a conductive material. The grids containing the sample sections can then be loaded onto a NanoSIMS sample holder, typically with a 10 mm diameter sub-holder designed to accommodate 3 TEM grids.

3.2.3 Fluorescence microscopy

In fluorescence microscopy, the sample is illuminated with light of a specific wavelength, which is then absorbed by the fluorophore present in the specimen. This absorption causes the fluorophore's energy level to transition from the ground state to an excited state. After a brief period in the excited state, the fluorophore returns to its ground state, emitting a photon of lower energy (longer wavelength) due to non-radiative energy losses, referred to as vibrational relaxation. This phenomenon is known as the Stokes shift. The molecular transitions that explain these phenomena can be visualized using Jablonski energy diagrams.[241]

A fluorescence microscope typically includes a primary light source, a series of refractive lenses, and a detector. The lenses are used to direct the light onto the sample. Scanning mirrors are employed to scan the light beam across the sample surface, with each scanned position representing a pixel in the final image. A dichroic mirror is used as a beam splitter to separate the excitation and emission light. This filter reflects light of a specific wavelength towards the sample, while allowing the emitted light from the sample to pass through towards the detector. The detector is specifically tuned to receive this emission wavelength and an image is produced based on the intensity of arriving photons and their location in the sample.[242]

Confocal microscopy is an optical fluorescence imaging technique that uses point illumination, and a pinhole allows only fluorescent signals produced very close to the focal plane to be detected (Figure 15A). Thus, the optical resolution is increased significantly compared to wide field where the entire sample is excited, resulting in a large unfocused background. Traditional confocal microscopy has a resolution limit of around 200 nm, which is sufficient for most biological applications. However, it faces challenges when it comes to imaging very small features below its resolution limit. Super-resolution techniques such as **stimulated emission depletion (STED) microscopy** can overcome the diffraction limit, achieving lateral resolution down to 20-50 nm.[243,244] STED operates by incorporating an additional depletion laser beam in a "donut shape" to restrict the area in which fluorophores can be in an "on" state, resulting in improved resolution.[245] Visual representation of the setup of a confocal / STED microscope are presented in Figure 15B.

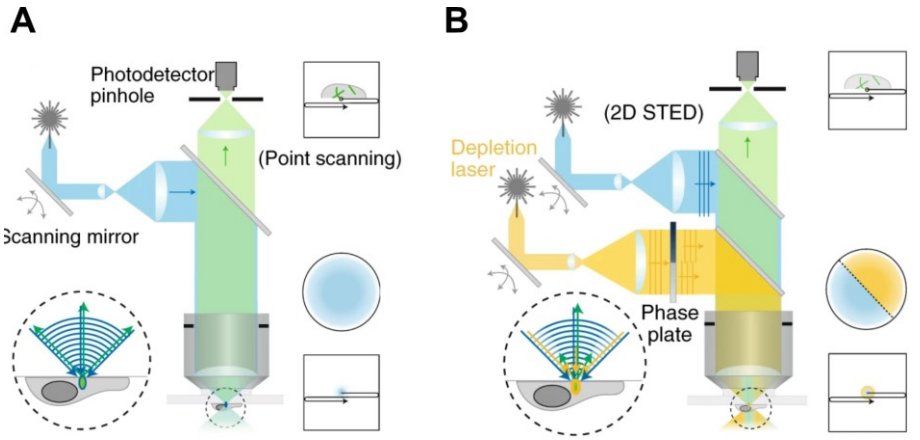

Figure 15. Schematic diagrams of confocal (**A**) and STED (**B**) microscopes. Reproduced with permission from reference [246].

Although confocal and STED microscopy do not match the resolution of electron microscopy or provide the same chemical information as in MSI, they offer advantages such as non-invasive optical sectioning, allowing examination of both living and fixed specimens with good contrast and resolution, and the ability for 3D imaging. This is particularly valuable for conducting live experiments, such as imaging live cells or isolated vesicles during electrochemical analysis, which will be discussed further in section 3.3. However, there are some disadvantages including the use of large fluorescent probes leading to image displacement, which can be reduced by using smaller tags like nanoprobes, or protein fusion tags. Photobleaching poses a challenge for both techniques, causing signal loss during sample preparation and imaging. Additionally, high-intensity laser irradiation can be harmful to living cells and tissues, particularly with STED microscopy.[247] To mitigate the issue, reducing the light dose during in-vivo imaging can be beneficial.

Fluorescent probes

There is a broad selection of labeling probes available, including fluorescent proteins, antibodies, nanobodies, and small-molecule fluorophores to name a few. Each type of probe possesses unique characteristics that make it suitable for different applications. These factors include color, size, fluorescence quantum yield, fluorescence decay time, and laser performance, among others.

Fluorescent proteins have been widely used as protein tags since the mid-1990s due to their high specificity and suitability for live cell experiments, although they do have certain limitations in their photophysical properties.[248,249] Another labeling approach involves the use of genetically-encoded protein tags combined with cell-permeable fluorescent ligands. These ligands offer increased brightness and are less susceptible to photobleaching compared to fluorescent proteins. Typically, both intrinsically and extrinsically fluorescent proteins are fused to a protein of interest (POI) to enable cellular imaging. To create a labeled version of a POI, a plasmid encoding the desired protein is often introduced into the cell through transfection, resulting in the expression of the target protein. For intrinsically fluorescent proteins like EGFP fluorescence occurs when three amino acid residues within a conserved β-barrel structure undergo cyclization and oxidation, leading to the formation of a two-ring chromophore (as depicted in Figure 16A).[250] In the case of extrinsically fluorescent proteins such as HaloTag (~33 kDa), the protein is initially non-fluorescent. Only when an appropriate activated fluorophore is added and binds to the HaloTag does it become fluorescent, as shown in Figure 16B.[251]

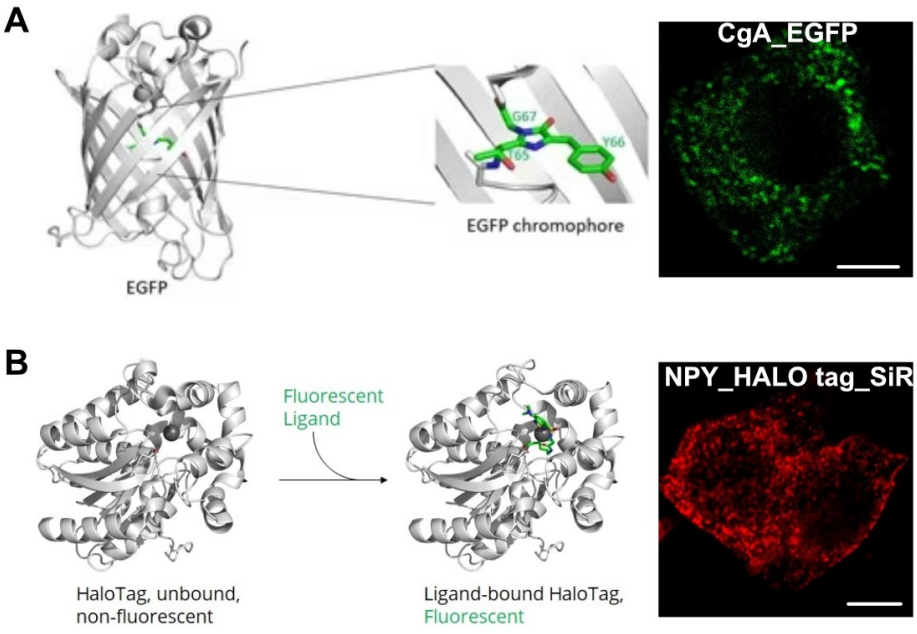

Figure 16. Illustration showcasing fluorescent probes used for monitoring exocytosis by targeting vesicular protein contents: (A) Enhanced GFP (EGFP), a derivative of GFP, displaying its β -barrel structure and fluorescent core with a magnified view of the two-ring chromophore; adjacent image depicts a PC12 cell expressing CgA-EGFP, enabling the detection of LDCVs. Scale bar: 5 µm. (B) Structure of apo-form HaloTag, displaying its basal conformation. Upon addition of an appropriate activated fluorophore, it is captured and covalently bound by the HaloTag residue D106, resulting in fluorescence; accompanying image portrays two PC12 cells expressing NPY-HaloTag, labeled with SiR. Scale bar: 5 µm. PDB IDs for structures: EGFP, 2y0g; apo-HaloTag, 5uy1; holo-HaloTag, 5uxz, adapted with permission from references [250,252].

Moreover, the pHluorin tag is worth mentioning due to its pH-sensitivity. It does not fluoresce under acidic conditions (pH < 6), but upon shifting to a physiological pH (7.4), it becomes intensely fluorescent.[253] By expressing the pHluorin tag in acidic secretory vesicles, it allows real-time analysis of exocytotic fusion events with the

plasma membrane. As the fusion pore opens and reaches a neutral pH, the fluorescence intensity significantly increases. Conversely, fusion pore closure is observed as a decrease in fluorescence when the vesicle's pH is restored. This capability enables investigation of fractional release modes such as kiss-and-run and partial release. Fluorescent forms of vesicle dense-core proteins, such as CgA-EGFP, are also commonly employed to track and observe the movement of vesicles (Figure 16A).[76] Neuropeptide Y (NPY) variants like NPY-EGFP, NPY-HaloTag, and NPY-pHluorin, are also used as indicators for LDCVs due to NPY co-storage with catecholamines in this type of vesicle.[111,254] Furthermore, synapto-pHluorin, a labeled version of synaptobrevin (a SNARE protein), can also be used to detect of both LDCVs and synaptic vesicles.[253]

An alternate approach for tracking specific types of vesicles involves labeling the content of vesicular neurotransmitters using small-molecule fluorophores. These include fluorescence-based turn-on sensors for primary amines, such as NeuroSensor 521 (NS521), and fluorescent false neurotransmitters (FFNs) such as FFN511, FFN102 and FFN270.[255–258] NS521 selectively recognizes norepinephrine and dopamine within secretory vesicles, leveraging their high concentration and the acidic environment, while showing no affinity for secondary amines like epinephrine (Figure 17A).[255] The FFNs typically incorporate a coumarin fluorophore scaffold and an aminoethyl group, resembling catecholamines. This structural similarity enables them to be actively transported across the plasma and vesicular membranes via specific transporters at neurons, as well as endocrine cells such as chromaffin and PC12 cells.[256,258]

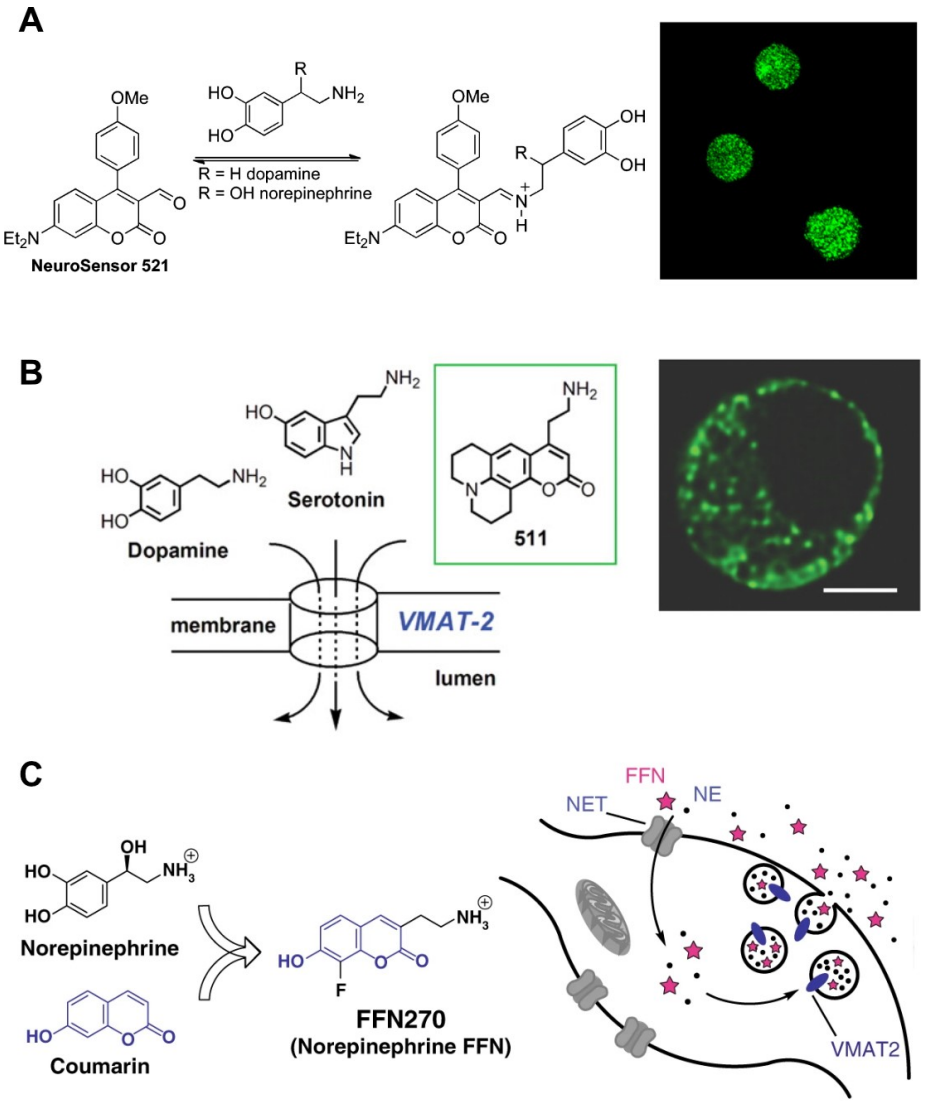

Figure 17. Illustration demonstrating the use of small-molecule fluorophores as optical tracers for neurotransmitters: (A) NeuroSensor521's working principle; on the right: an image of chromaffin cells containing norepinephrine, incubated with NS521 (0.1 μM). Adapted with permission from reference [255]. (B) FN511's working principle; on the right: a multiphoton image of a chromaffin cell showing FFN511 distribution consistent with LDCVs. Scale bar, 5 μm. Reproduced with permission from reference [256]. (C) FFN270's

working principle; on the right: NE-FFNs track the uptake of norepinephrine from the extracellular space, its packaging into vesicles, and subsequent exocytosis as they are designed to be substrates for NET and VMAT2. Reproduced with permission from reference [258].

Among the FFNs, FFN511 functions as a substrate for the vesicular monoamine transporter (VMAT2). Consequently, after being taken up from the extracellular space, FFN511 is packaged into vesicles in a manner similar to native monoamine neurotransmitters and can subsequently undergo exocytosis.[259] Likewise, FFN102, a dopaminergic FFN, acts as a substrate for both the plasma membrane dopamine transporter (DAT) and VMAT2. FFN270 follows a similar mechanism; however, it serves as a fluorescent substrate for the norepinephrine transporter (NET) while also being a substrate for VMAT2. The utilization of fluorescence microscopy with FFNs provides a strategy for tracking exocytosis as shown in Figure 17B-C.

In addition to targeting the contents of vesicles, another approach to monitor vesicular transport processes like exocytosis, endocytosis, and recycling of vesicles involves labeling the lipid membrane. There are several options available for this purpose. Some examples include the styryl dye FM1-43, the membrane-binding fluorophore-cysteine-lysine-palmitoyl group (mCLING), and fluorescent phospholipids. FM1-43, for example, can reversibly bind to the outer leaflet of the surface membrane and be taken up during endocytosis, resulting in the staining of newly formed vesicles. When these labeled vesicles undergo exocytosis in a dye-free medium, FM1-43 molecules dissociate from the membrane, causing the loss of fluorescence.[260] Similarly, mCLING also labels the plasma membrane and is absorbed during endocytosis (Figure

18A). However, it remains attached to the membranes even after fixation and permeabilization, making it suitable for use in combination with immunostaining. Additionally, mCLING can be coupled with Atto647N dye, making it ideal for stimulated emission depletion (STED) microscopy.[261] Fluorescent phospholipids that have a labeled head group can be utilized to introduce fluorescence into the plasma membrane, thereby facilitating the visualization of the vesicles.[262,263] Although labeling the lipid membrane is not specific to vesicles alone, it has the potential to label other membrane organelles as well. Therefore, it is recommended to also use a more targeted label for accurate identification of the vesicles. In **paper IV**, FFN511 was combined with the membrane label Rhod PE (Figure 18B) to label isolated chromaffin vesicles.

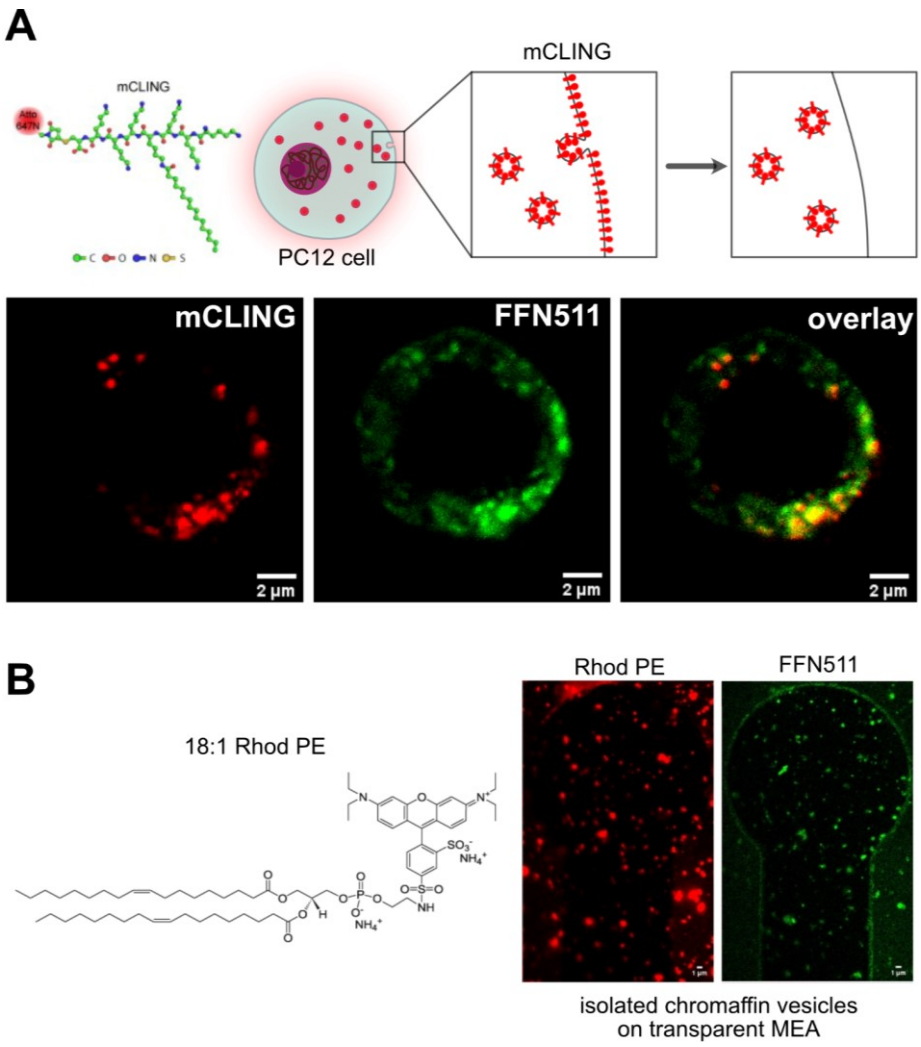

Figure 18. Illustration demonstrating the use of membrane probes for tracking vesicles: (A) The structure and working principle of mCLING, adapted and recreated base on reference [261]. The lower panel illustrates mCLING labeling of the vesicle membrane in live PC12 cells through high potassium stimulation to evoke exocytosis-endocytosis. The cells were then incubated with FFN511 to also label the vesicle content. (B) The structure of Rhod PE. On the right side, isolated chromaffin vesicles are labeled with FFN511 and Rhod PE.

3.3 Electrochemical analysis

Electroanalytical methods involve studying how electrons move between an electrode surface and an analyte in a solution. This happens in the presence of an electrolyte. For instance, a reversible charge transfer reaction occurs at the working electrode, where a species (Ox) can be reduced to form another species (Red) by accepting n electrons (e^-) from the working electrode:

$$Ox + ne^- \leftrightarrow Red$$

An equilibrium condition is reached when the net flux of all species is zero; and the electrode reaches a certain electric potential. This potential is measured as a difference between two electrodes in the solution. One electrode is chosen as a reference, and measurements on the working electrode are compared to this reference.

Voltammetric methods include a set of techniques that operate under non-equilibrium conditions. In these methods, a potential is applied to a working electrode that is placed in an electrolyte solution, and the resulting current is examined. By adjusting the applied potential to be more negative or more positive than the equilibrium potential, it becomes possible to manipulate the reaction towards either the oxidized or reduced state of the substance. One specific technique within voltammetry is called amperometry. In amperometry, a constant potential is initially applied between the working electrode and the reference electrode. As the experiment progresses, the current is observed over time, allowing changes in the concentration of the analyte to be monitored, which are seen as fluctuations in the current.

3.3.1 Single cell amperometry

Electrochemical measurements of single cells have been reported as early as the 1980s, when carbon microelectrodes were utilized to measure the concentration of serotonin using intracellular voltammetry.[264] Moving forward to the early 1990s, the Wightman group introduced a new method called amperometry. They employed disk-shaped microelectrodes to study exocytotic release events that occur in single bovine chromaffin cells.[265] Through the combination of amperometry with cyclic voltammetry, later, they were able to confirm that the detected release events are oxidized catecholamine molecules.[132]

Single cell amperometry (SCA) allows direct quantification of exocytotic release of electroactive neurotransmitters. The release events are often triggered by external stimuli, causing an increase in the intracellular Ca^{2+} concentration initiating vesicle fusion. Electroactive neurotransmitters, including dopamine, norepinephrine, epinephrine, serotonin, among others, can be either oxidized or reduced within a specific range of potentials. Thus, the experimental setup of SCA involves a stimulation pipette and a microelectrode held at a sufficient overpotential, positioned on top of a living cell. When the released neurotransmitters reach the electrode surface, they are immediately oxidized, resulting in a current response over time, known as a spike (Figure 19A-B). By employing a high sampling rate, individual exocytotic release events can be detected, with each spike corresponding to the exocytosis from a single vesicle, as depicted in Figure 19C-1. Analyzing the characteristics of these spikes provides valuable information about the dynamics of the release event. The rise time (t_{rise}) typically reflects the expansion of the fusion pore, while the fall time

(t_{fall}) represents the closing of the pore and the clearance of released molecules from the extracellular space. The amplitude of the spike (I_{max}) describes the maximum flux of molecules, and the full width at half maximum ($t_{1/2}$) indicates the overall duration of the event (Figure 19B). Additionally, the number of molecules released can be quantified based on the charge (Q). The charge (Q) is directly proportional to the number of moles (N) released during the event, as described by Faraday's law (equation 4). In this equation, *n* represents the number of electrons transferred during the reaction (n = 2 electrons for catecholamines), and *F* is the Faraday constant (F = 96485 $Cmol^{-1}$). The number of molecules released during the event can be calculated by simply multiplying the number of moles (N) with Avogadro's number ($N_A = 6.022 \times 10^{23}$).

$$N = \frac{Q}{nF} \tag{4}$$

While amperometry is quantitative and exhibits excellent temporal resolution, high sensitivity, it does have limitations in terms of selectivity. In the case of catecholamine transmitters, namely dopamine, norepinephrine, and epinephrine, their similar structural characteristics also result in similar oxidation potentials. Consequently, it becomes challenging to specifically measure one of these neurotransmitters without interference from the other two. A proposed method for distinguishing secretory granules containing epinephrine from other catecholamines in chromaffin cells is by using fast-scan cyclic voltammetry.[266] Although, it is worth noting that, PC12 cell vesicles predominantly contain dopamine, with only minimal amounts of norepinephrine.[162] This observation allows us to make an assumption that the majority of the measured catecholamines are likely dopamine.

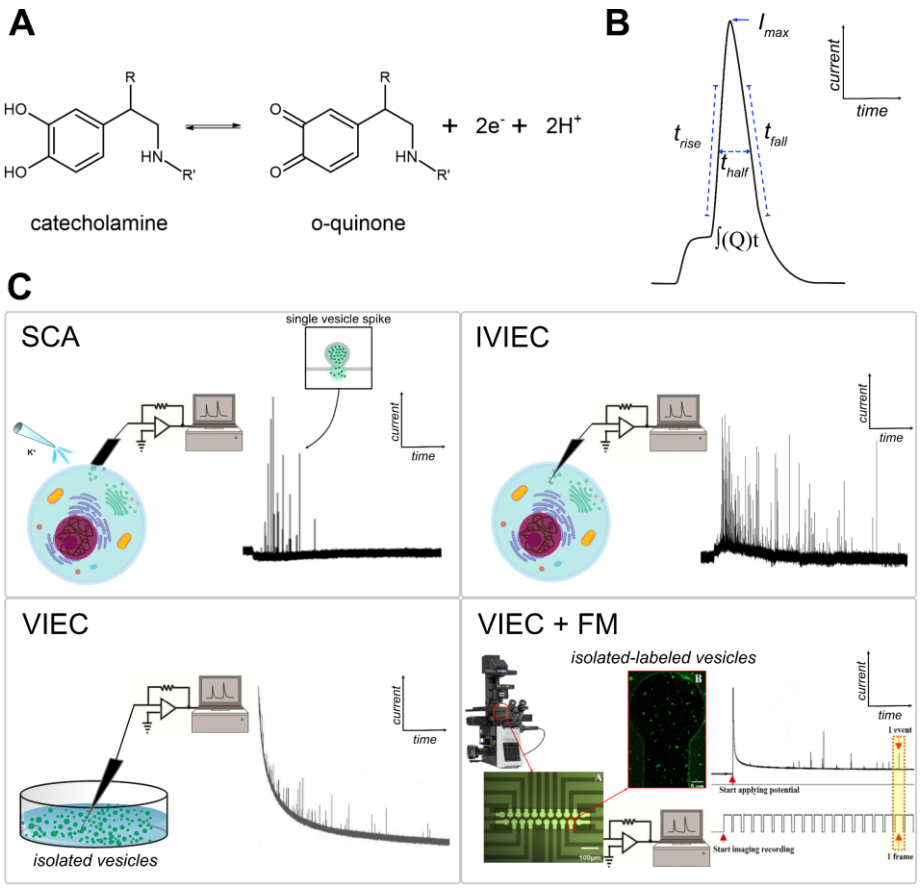

Figure 19. Overview of some electrochemical techniques used in the study of exocytosis. (A) Redox reactions of catecholamines. (B) Illustration of a spike showing relevant parameters of an amperometric spike. (C) Schematic representation of different setups: (1) SCA setup, where a disk microelectrode is placed on top of the cell and exocytosis is stimulated using a pipette containing high concentration K^+; (2) IVIEC measurement, achieved by gently inserting a nanotip electrode into a single living cell; (3) conventional VIEC measurement of an isolated vesicle suspension; (4) VIEC measurement combined with fluorescence imaging using transparent multi-electrode arrays (MEAs), where the isolated vesicles are fluorescently labeled.

Since its invention in the 1990s, SCA has been extensively utilized for studying the fundamentals of exocytosis. This technique has played a crucial role in quantifying catecholamine release from LDCVs in PC12 cells and from SVs in cultured neurons.[133,267,268] Moreover, amperometry has been applied in the investigations of the co-release of catecholamines and ATP from the same vesicles in chromaffin cells.[269] In addition to catecholamines, studies have successfully reported norepinephrine, serotonin, and octopamine release in different biological models.[269–271] These findings highlight the versatility and wide applicability of amperometry.

3.3.2 Vesicle Impact Electrochemical Cytometry and Intracellular Vesicle Impact Electrochemical Cytometry

While SCA provides important information about the release amount, quantifying the full vesicular content is crucial to fully understand the whole release process. In 2015, the Ewing group developed two analytical methods, namely vesicle impact electrochemical cytometry (VIEC) and intracellular vesicle impact electrochemical cytometry (IVIEC).[79,131] In VIEC, an electrode is typically placed in a concentrated vesicle suspension, while in IVIEC, a carbon fiber electrode with a sharp tip is used to penetrate into the cytoplasm of a living cell, enabling quantification of individual vesicle content within the cell (see Figures 19C2-3). VIEC allows the determination of total vesicle content in isolated vesicles, while IVIEC enables quantification of the content of individual vesicles within living cells. By combining these techniques with SCA, the fraction of release can be calculated by comparing the amount of released transmitter to the amount stored, revealing that only a fraction of a secretory vesicle's cargo is released during exocytosis.

The exact mechanisms involved in these two techniques, specifically how vesicles rupture and open to enable transmitter quantification by the electrodes, are not yet fully understood. However, it has been suggested that applying a potential to the electrode can induce electroporation in the vesicle membrane, creating a pore through which transmitters diffuse and are detected.[272] The frequency of vesicle rupture has been shown to increase by higher potential or temperature.[273] Additionally, larger vesicles tend to rupture more easily and earlier compared to smaller ones.[263]

Despite the similarities between VIEC and IVIEC, they have distinct applications when it comes to studying vesicles. In IVIEC, the cell remains intact, enabling the monitoring of intracellular vesicles under external factors such as osmolarity, pH, and pharmaceutical treatments. On the other hand, VIEC isolates vesicles from cells, allowing the transfer of vesicles to a different environment. This characteristic makes it convenient for directly manipulating the loading process of vesicles and labeling them for further analysis.

A combination of VIEC with confocal microscopy was employed in **paper IV** to observe the process of labeled vesicles opening on the electrode surface for better understanding of the mechanism involve in VIEC.[263] To carry out this observation, a transparent Au/ITO microelectrode (5 nm thick, 33 μm in diameter) in a 20x2 multi-electrode array (MEA) was used. This MEA served as both an electrode for VIEC and a clear surface for confocal imaging. This hybrid method allowed optical and electrochemical measurements of single vesicles (Figure 19C-4).

Chapter 4. Summary of papers

This thesis aims to enhance our understanding of the mechanisms and characteristics of vesicular content release, with a specific focus on partial release. Multiple techniques were integrated to comprehensively explore this process and quantitatively evaluate the release fraction.

Paper I focused on visualizing large dense core vesicles (LDCVs) of PC12 cells that were treated with isotopically labeled L-DOPA. The ^{13}C labeled L-DOPA was taken up by the cells, synthesized into dopamine, and loaded into LDCVs via membrane transporters. The cellular and vesicular ultrastructure were observed using TEM, detection and localization of the labeled dopamine was carried out with NanoSIMS. The dense core and halo compartments of LDCVs were distinguished by pushing the high spatial resolution of NanoSIMS. This study found that labeled dopamine was preferentially stored in the dense cores of LDCVs, and the local concentration of dopamine was quantified.

In **paper II**, correlative TEM and NanoSIMS imaging were employed to visualize vesicles undergoing partial release in PC12 cells. The cellular vesicles were loaded with isotopically labeled L-DOPA, and a second marker (a molecule containing ^{127}I) was exposed to the external environment of the cells during exocytosis. This allowed the marker to diffuse into the vesicles through the transiently open exocytotic pore before closure. The vesicles undergoing partial release were identified, which exhibited a decrease in size and reduced levels of ^{13}C labeled dopamine, but increased levels of ^{127}I. The fraction of neurotransmitter release was determined through $\delta^{13}C‰$ and size measurements. The

colocalization of the ^{13}C and ^{127}I signals suggested molecular movement into and out of the vesicles during partial release.

Paper III expanded on the duo-label approach to explore the role of vesicle size in partial release dynamics. Correlative TEM and NanoSIMS were employed to study PC12 cells that had been genetically modified to alter the size of their LDCVs. We observed vesicle size changes through TEM imaging and then localized and quantified the isotopically labeled dopamine using NanoSIMS. The findings indicated that the fraction of release in partial release events did not correlate with vesicle size under specific experimental conditions. This suggests that partial release can occur across a wide range of vesicle sizes.

Paper IV introduced a hybrid method, combining vesicle impact electrochemical cytometry (VIEC) and live confocal imaging. This approach allowed simultaneous analysis and location of vesicular content release. Chromaffin vesicles from the bovine adrenal medulla were isolated and fluorescently labeled for both neurotransmitters and vesicle membranes. A transparent multielectrode array was developed to serve as both an electrode for VIEC and a suitable surface for confocal microscopy. Three distinct opening patterns correlating with vesicle content and size were observed by imaging the vesicles during the opening process on the electrode surface, and adsorption and residence times were evaluated.

Chapter 5. Concluding remarks & future outlook

Cellular communication is vital for maintaining normal physiological processes. The intricate process of exocytosis plays a crucial role in facilitating efficient communication between cells. The focus of this work has been on the development of quantitative chemical imaging approaches to expand our understanding of vesicular content release from different perspectives. Methodology for combining mass spectrometry imaging with electron microscopy or electrochemical analysis and fluorescence microscopy have been described. The strengths and weaknesses of each technique, as well as effective and practical methods for integrating them in the study of neurotransmitters release, have been discussed.

The results demonstrate that correlative TEM and NanoSIMS imaging can be used to effectively localize and quantify labeled dopamine distributions at the subvesicular level. By utilizing a dual labeling method, partially released vesicles can be visualized, uncovering molecular movement in and out of nanovesicles during the process of partial release. Similar fractions of release were observed across a range of vesicle sizes, suggesting the ubiquity of this mode of exocytosis. Overall, these integrated techniques enable visualization and quantification of nanovesicle contents as well as measurement of release fractions. These capabilities hold the potential to provide valuable insights into the mechanisms underlying exocytosis and how it may be affected in different disease states or in response to specific pharmaceutical treatments. The research can be expanded, for example, by delving further into the investigation of different types of

neurotransmitters released from various biological models, including other secretory cells and primary neurons. Additionally, the availability of innovative technologies like cryoNanoSIMS allow maintaining the samples even closer to their native state, potentially enabling more accurate observations. However, operating at very low temperatures, as required by cryogenic methods, may have an impact on the ionization efficiency of the samples (i.e., lower count).[176] The described dual labeling method holds the potential for further investigation into the close coupling of exo-endocytosis and/or vesicle retrieval.

The work in this thesis also presents an approach for combining electrochemical techniques and live confocal imaging. This was achieved through the development of transparent MEAs, which allow real-time analysis of vesicular content release from isolated vesicles. This MEAs design also holds promise for single cell analysis. Further advances can be made by exploring different electrode materials or by modifying the MEA geometry to withstand the interference from strong depletion lasers, enabling the coupling of electrochemical analysis with stimulated emission depletion microscopy.[274] Another alternative is to combine amperometry methods with TIRFM, in order to enhance spatial and temporal resolution and mitigate the interference of strong depletion lasers on both the electrode and the living cell.[275]

Acknowledgments

I want to express my sincere gratitude to my main supervisor, **Andrew Ewing**, for giving me the opportunity to pursue a PhD in this incredible environment. Your support and mentorship have been invaluable, allowing me to explore and learn from both successes and failures. The personal and professional growth I have experienced throughout this journey is something I will forever cherish. I would also like to extend my sincere appreciation to my second supervisor, **Nhu Phan**. Thank you for your continuous support and for involving me in many exciting projects with your group. To my third supervisor, **Michael Kurczy**, I am immensely grateful for all your invaluable advice and support. The energy and excitement you bring to every discussion, particularly regarding NanoSIMS, is truly inspiring. Furthermore, I would like to acknowledge my examiner, **Sebastian Westenhoff**, for keeping track of my PhD progress throughout the years. To all my **co-authors**, thanks for the opportunity to work together with you. Our collaborations have not only been productive but also enjoyable. And thanks to all the **funding agencies** without whom this work would not have been possible.

To **Alicia Lork**, **Stefania Rabasco**, and **Kim Long Le Vo**, your care and friendship mean so much to me! Sharing this wild ride with lab mates as dedicated and fun as you all is an absolute blessing. To **Andre Du Toit**, thank you for always being so helpful and approachable. Your passion for science is seriously inspiring. I also want to thank **Chaoyi Gu**, **Kelly D. Nilsson**, **Mai H. Philipsen**, and **Anna Larsson** for helping me out in the early days of my PhD. Our adventures together as travel buddies are fantastic memories. And to **Alex S. Lima**, **Xinwei Zhang**,

and **Soodabeh Majdi**, thank you for sharing your knowledge of electrochemistry and engaging in many great discussions. To **Johan Dunevall** and **Peter Oomen**, thank you for sharing your expertise in microfabrication and for the enjoyable time we spent working together in the cleanroom. I am also grateful to **Aurélien Thomen** for sharing your knowledge of the NanoSIMS. And **Elias Ranjbari**, thank you for your tremendous support at the Chemical Imaging Infrastructure. I would like to acknowledge the Centre for Cellular Imaging at the University of Gothenburg and the National Microscopy Infrastructure for providing assistance in electron microscopy. I also want to express my gratitude to all **the present and former students and staff of Analytical Chemistry at GU and Chalmers**. Once again, I want to thank each and every one of you for your kindness and support. This journey would not have been the same without you!

To my **family** and **extended family**, your care means the world to me! Whether offering a helping hand or simply being there for me, you always make me feel like I am home no matter what. *Cảm ơn mẹ rất nhiều!*

To **Johan**, thank you for being beyond supportive all these years. You are the absolute best! And to my **kiddos**, you have reminded me every single day to give my all, work harder, and stay focused on my dreams. Thank you all for your love and encouragement!

References

(1) Armingol, E.; Officer, A.; Harismendy, O.; et al. Deciphering Cell–Cell Interactions and Communication from Gene Expression. *Nat. Rev. Genet.* **2021**, *22*, 71–88.

(2) Rudnick, G.; Clark, J. From Synapse to Vesicle: The Reuptake and Storage of Biogenic Amine Neurotransmitters. *Biochim. Biophys. Acta* **1993**, *1144*, 249–263.

(3) Wong, D. L. Epinephrine Biosynthesis: Hormonal and Neural Control During Stress. *Cell. Mol. Neurobiol.* **2006**, *26*, 889–898.

(4) Axelrod, J.; Reisine, T. D. Stress Hormones: Their Interaction and Regulation. *Science* **1984**, *224*, 452–459.

(5) Byrne, C. J.; Khurana, S.; Kumar, A.; et al. Inflammatory Signaling in Hypertension: Regulation of Adrenal Catecholamine Biosynthesis. *Front. Endocrinol. (Lausanne).* **2018**, *9*, 1–25.

(6) Newton, A. C.; Bootman, M. D.; Scott, J. D. Second Messengers. *Cold Spring Harb. Perspect. Biol.* **2016**, *8*.

(7) García, A. G.; García-De-Diego, A. M.; Gandía, L.; et al. Calcium Signaling and Exocytosis in Adrenal Chromaffin Cells. *Physiol. Rev.* **2006**, *86*, 1093–1131.

(8) Neher, E.; Sakaba, T. Multiple Roles of Calcium Ions in the Regulation of Neurotransmitter Release. *Neuron* **2008**, *59*, 861–872.

(9) Kandel, E. R.; Schwartz, J. H.; Jessell, T. M.; et al. *Principles of Neural Science*; 5th ed.; McGraw-hill New York, 2013; Vol. 4.

(10) Mahata, S. K.; Corti, A. Chromogranin a and Its Fragments in Cardiovascular, Immunometabolic, and Cancer Regulation. *Ann. N. Y. Acad. Sci.* **2019**, *1455*, 34–58.

(11) Rienecker, K. D. A.; Poston, R. G.; Saha, R. N. Merits and Limitations of Studying Neuronal Depolarization-Dependent Processes Using Elevated External Potassium. *ASN Neuro* **2020**, *12*, 1–17.

(12) Purves D, Augustine GJ, Fitzpatrick D, et al. What Defines a Neurotransmitter? In *Neuroscience*; Sunderland (MA): Sinauer Associates, 2001.

(13) Esplugues, J. V. NO as a Signalling Molecule in the Nervous System. *Br. J. Pharmacol.* **2002**, *135*, 1079–1095.

(14) Paul, B. D.; Snyder, S. H. H2S: A Novel Gasotransmitter That Signals by Sulfhydration. *Trends Biochem. Sci.* **2015**, *40*, 687–700.

(15) Purves D, Augustine GJ, Fitzpatrick D, et al. Chapter 6, Neurotransmitters. In *Neuroscience.*; Sunderland (MA): Sinauer Associates, 2001.

(16) Purves D, Augustine GJ, Fitzpatrick D, et al., E. Two Major Categories of Neurotransmitters. In *Neuroscience*; Sunderland (MA): Sinauer Associates, 2001.

(17) Hyman, S. E. Neurotransmitters. *Curr. Biol.* **2005**, *15*, 154–158.

(18) Luykx, J. J.; Laban, K. G.; van den Heuvel, M. P.; et al. Region and State Specific Glutamate Downregulation in Major Depressive Disorder: A Meta-Analysis of 1H-MRS Findings. *Neurosci. Biobehav. Rev.* **2012**, *36*, 198–205.

(19) Pehrson, A. L.; Sanchez, C. Altered γ-Aminobutyric Acid Neurotransmission in Major Depressive Disorder: A Critical Review of the Supporting Evidence and the Influence of Serotonergic Antidepressants. *Drug Des. Devel. Ther.* **2015**, *9*, 603–624.

(20) Conio, B.; Martino, M.; Magioncalda, P.; et al. Opposite Effects of Dopamine and Serotonin on Resting-State Networks: Review and Implications for Psychiatric Disorders. *Mol. Psychiatry* **2020**, *25*, 82–93.

(21) Hamon, M.; Blier, P. Monoamine Neurocircuitry in Depression and Strategies for New Treatments. *Prog. Neuro-Psychopharmacology Biol. Psychiatry* **2013**, *45*, 54–63.

(22) Lyon, G. J.; Abi-Dargham, A.; Moore, H.; et al. Presynaptic Regulation of Dopamine Transmission in Schizophrenia. *Schizophr. Bull.* **2011**, *37*, 108–117.

(23) Nutt, D. J.; Lingford-Hughes, A.; Erritzoe, D.; et al. The Dopamine Theory of

Addiction: 40 Years of Highs and Lows. *Nat. Rev. Neurosci.* **2015**, *16*, 305–312.
(24) Triarhou, L. C. Dopamine and Parkinson's Disease. In *Madame Curie Bioscience Database*; Landes Bioscience, 2013.
(25) Blum, K.; Chen, A. L.-C.; Braverman, E. R.; et al. Attention-Deficit-Hyperactivity Disorder and Reward Deficiency Syndrome. *Neuropsychiatr. Dis. Treat.* **2008**, *4*, 893–918.
(26) Cepeda, C.; Murphy, K. P. S.; Parent, M.; et al. The Role of Dopamine in Huntington's Disease. *Prog. Brain Res.* **2014**, *211*, 235–254.
(27) Kumar, A.; Nisha, C. M.; Silakari, C.; et al. Current and Novel Therapeutic Molecules and Targets in Alzheimer's Disease. *J. Formos. Med. Assoc.* **2016**, *115*, 3–10.
(28) Brichta, L.; Greengard, P.; Flajolet, M. Advances in the Pharmacological Treatment of Parkinson's Disease: Targeting Neurotransmitter Systems. *Trends Neurosci.* **2013**, *36*, 543–554.
(29) Seidah, N. G.; Chrétien, M. Proprotein and Prohormone Convertases: A Family of Subtilases Generating Diverse Bioactive Polypeptides. *Brain Res.* **1999**, *848*, 45–62.
(30) Mains, R. E.; Cullen, E. I.; May, V.; et al. The Role of Secretory Granules in Peptide Biosynthesis. *Ann. N. Y. Acad. Sci.* **1987**, *493*, 278–291.
(31) Hökfelt, T.; Barde, S.; Xu, Z.-Q. D.; et al. Neuropeptide and Small Transmitter Coexistence: Fundamental Studies and Relevance to Mental Illness. *Frontiers in Neural Circuits*, 2018, *12*.
(32) Strand, F. L. *Neuropeptides: Regulators of Physiological Processes*; MIT press, 1999.
(33) Gorman, B. L.; Brunet, M. A.; Pham, S. N.; et al. Measurement of Absolute Concentration at the Subcellular Scale. *ACS Nano* **2020**, *14*, 6414–6419.
(34) Takiyyuddin, M. A.; Brown, M. R.; Dinh, T. Q.; et al. Sympatho-adrenal Secretion in Humans: Factors Governing Catecholamine and Storage Vesicle Peptide Co-release. *J. Auton. Pharmacol.* **1994**, *14*, 187–200.
(35) Merten, N.; Beck-Sickinger, A. G. Molecular Ligand-Receptor Interaction of the NPY/PP Peptide Family. *NPY Fam. Pept. Neurobiol. Cardiovasc. Metab. Disord. from Genes to Ther.* **2006**, *95*, 35–62.
(36) Renshaw, D.; Thomson, L. M.; Carroll, M.; et al. Actions of Neuropeptide Y on the Rat Adrenal Cortex. *Endocrinology* **2000**, *141*, 169–173.
(37) Shimoda, K.; Shen, G. H.; Pfeiffer, R. F.; et al. Antiserum against Neuropeptide Y Enhances the Nicotine-Mediated Release of Catecholamines from Cultured Rat Adrenal Chromaffin Cells. *Neurochem. Int.* **1993**, *23*, 71–77.
(38) Higuchi, H.; Costa, E.; Yang, H. Y. Neuropeptide Y Inhibits the Nicotine-Mediated Release of Catecholamines from Bovine Adrenal Chromaffin Cells. *J. Pharmacol. Exp. Ther.* **1988**, *244*, 468–474.
(39) Carlsson, A. A Paradigm Shift in Brain Research. *Science (80-.).* **2001**, *294*, 1021–1024.
(40) Bromberg-Martin, E. S.; Matsumoto, M.; Hikosaka, O. Dopamine in Motivational Control: Rewarding, Aversive, and Alerting. *Neuron* **2010**, *68*, 815–834.
(41) Gepshtein, S.; Li, X.; Snider, J.; et al. Dopamine Function and the Efficiency of Human Movement. *J. Cogn. Neurosci.* **2014**, *26*, 645–657.
(42) Cavallotti, C.; Mancone, M.; Bruzzone, P.; et al. Dopamine Receptor Subtypes in the Native Human Heart. *Heart Vessels* **2010**, *25*, 432–437.
(43) Ozono, R.; O'Connell, D. P.; Wang, Z. Q.; et al. Localization of the Dopamine D1 Receptor Protein in the Human Heart and Kidney. *Hypertension* **1997**, *30*, 725–729.
(44) Martel, J. C.; Gatti McArthur, S. Dopamine Receptor Subtypes, Physiology and Pharmacology: New Ligands and Concepts in Schizophrenia. *Front. Pharmacol.* **2020**, *11*.
(45) Mishra, A.; Singh, S.; Shukla, S. Physiological and Functional Basis of Dopamine Receptors and Their Role in Neurogenesis: Possible Implication for Parkinson's

Disease. *J. Exp. Neurosci.* **2018**, *12*.
(46) Feher, J. Cells, Synapses, and Neurotransmitters. In *Quantitative Human Physiology (Second Edition)*; Academic Press: Boston, 2012; pp. 375–388.
(47) Archer, M.; Dogra, N.; Dovey, Z.; et al. Role of α- and β-Adrenergic Signaling in Phenotypic Targeting: Significance in Benign and Malignant Urologic Disease. *Cell Commun. Signal.* **2021**, *19*, 78.
(48) Taegtmeyer, H.; Ganim, J.; Leuppi-Taegtmeyer, A. B. Hermann ("Hugh") Blaschko (1900–1993): Father of Catecholamine Metabolism. *Cardiology* **2023**, *148*, 93–97.
(49) Sandler, M.; Ruthven, C. R. J. The Biosynthesis and Metabolism of the Catecholamines. *Prog. Med. Chem.* **1969**, *6*, 200–265.
(50) Anderson, D. J.; Michelsohn, A. Role of Glucocorticoids in the Chromaffin-neuron Developmental Decision. *Int. J. Dev. Neurosci.* **1989**, *7*, 475–483.
(51) Berends, A. M. A.; Eisenhofer, G.; Fishbein, L.; et al. Intricacies of the Molecular Machinery of Catecholamine Biosynthesis and Secretion by Chromaffin Cells of the Normal Adrenal Medulla and in Pheochromocytoma and Paraganglioma. *Cancers (Basel).* **2019**, *11*, 1121.
(52) Loizou, L. A. Effect of Inhibition of Catecholamine Synthesis on Central Catecholamine-Containing Neurones in the Developing Albino Rat. *Br. J. Pharmacol.* **1971**, *41*, 41–48.
(53) Christenson, J. G.; Dairman, W.; Udenfriend, S. Preparation and Properties of a Homogeneous Aromatic L-Amino Acid Decarboxylase from Hog Kidney. *Arch. Biochem. Biophys.* **1970**, *141*, 356–367.
(54) Vendelboe, T. V; Harris, P.; Zhao, Y.; et al. The Crystal Structure of Human Dopamine β-Hydroxylase at 2.9 Å Resolution. *Sci. Adv.* **2016**, *2*, e1500980.
(55) Terland, O.; Flatmark, T. Ascorbate as a Natural Constituent of Chromaffin Granules from the Bovine Adrenal Medulla. *FEBS Lett.* **1975**, *59*, 52–56.
(56) Zuckerman-Levin, N.; Tiosano, D.; Eisenhofer, G.; et al. The Importance of Adrenocortical Glucocorticoids for Adrenomedullary and Physiological Response to Stress: A Study in Isolated Glucocorticoid Deficiency. *J. Clin. Endocrinol. Metab.* **2001**, *86*, 5920–5924.
(57) Kalaria, R. N.; Mitchell, M. J.; Harik, S. I. Monoamine Oxidases of the Human Brain and Liver. *Brain* **1988**, *111*, 1441–1451.
(58) Cesura, A. M. Monoamine Oxidases. *xPharm Compr. Pharmacol. Ref.* **2007**, 1–5.
(59) Chen, J.; Lipska, B. K.; Halim, N.; et al. Functional Analysis of Genetic Variation in Catechol-O-Methyltransferase (COMT): Effects on MRNA, Protein, and Enzyme Activity in Postmortem Human Brain. *Am. J. Hum. Genet.* **2004**, *75*, 807–821.
(60) Tenhunen, J.; Salminen, M.; Jalanko, A.; et al. Structure of the Rat Catechol-O-Methyltransferase Gene: Separate Promoters Are Used to Produce MRNAs for Soluble and Membrane-Bound Forms of the Enzyme. *DNA Cell Biol.* **1993**, *12*, 253–263.
(61) Kopin, I. J. Catecholamine Metabolism: Basic Aspects and Clinical Significance. *Pharmacol. Rev.* **1985**, *37*, 333–364.
(62) Qu, L.; Akbergenova, Y.; Hu, Y.; et al. Synapse-to-Synapse Variation in Mean Synaptic Vesicle Size and Its Relationship with Synaptic Morphology and Function. *J. Comp. Neurol.* **2009**, *514*, 343–352.
(63) Jahn, R.; Südhof, T. C. Synaptic Vesicle Traffic: Rush Hour in the Nerve Terminal. *J. Neurochem.* **1993**, *61*, 12–21.
(64) Schikorski, T.; Stevens, C. F. Quantitative Ultrastructural Analysis of Hippocampal Excitatory Synapses. *J. Neurosci. Off. J. Soc. Neurosci.* **1997**, *17*, 5858–5867.
(65) Dean, P. M. Ultrastructural Morphometry of the Pancreatic β-Cell. *Diabetologia* **1973**, *9*, 115–119.
(66) Jia, X. X.; Gorczyca, M.; Budnik, V. Ultrastructure of Neuromuscular Junctions in Drosophila: Comparison of Wild Type and Mutants with Increased Excitability. *J.*

Neurobiol. **1993**, *24*, 1025–1044.

(67) Plattner, H.; Artalejo, A. R.; Neher, E. Ultrastructural Organization of Bovine Chromaffin Cell Cortex-Analysis by Cryofixation and Morphometry of Aspects Pertinent to Exocytosis. *J. Cell Biol.* **1997**, *139*, 1709–1717.

(68) Kim, T.; Tao-Cheng, J.-H.; Eiden, L. E.; et al. Chromogranin A, an "On/Off" Switch Controlling Dense-Core Secretory Granule Biogenesis. *Cell* **2001**, *106*, 499–509.

(69) Maneu, V.; Borges, R.; Gandía, L.; et al. Forty Years of the Adrenal Chromaffin Cell through ISCCB Meetings around the World. *Pflugers Arch. Eur. J. Physiol.* **2023**, *475*, 667–690.

(70) Patzak, A.; Winkler, H. Exocytotic Exposure and Recycling of Membrane Antigens of Chromaffin Granules: Ultrastructural Evaluation after Immunolabeling. *J. Cell Biol.* **1986**, *102*, 510–515.

(71) Dembla, E.; Becherer, U. Biogenesis of Large Dense Core Vesicles in Mouse Chromaffin Cells. *Traffic* **2021**, *22*, 78–93.

(72) Estevez-Herrera, J.; Pardo, M. R.; Dominguez, N.; et al. The Role of Chromogranins in the Secretory Pathway. *Biomol. Concepts* **2013**, *4*, 605–609.

(73) Rudolf, R.; Salm, T.; Rustom, A.; et al. Dynamics of Immature Secretory Granules: Role of Cytoskeletal Elements during Transport, Cortical Restriction, and F-Actin-Dependent Tethering. *Mol. Biol. Cell* **2001**, *12*, 1353–1365.

(74) Takamori, S.; Holt, M.; Stenius, K.; et al. Molecular Anatomy of a Trafficking Organelle. *Cell* **2006**, *127*, 831–846.

(75) Viveros, O. H.; Wilson, S. P. The Adrenal Chromaffin Cell as a Model to Study the Co-Secretion of Enkephalins and Catecholamines. *J. Auton. Nerv. Syst.* **1983**, *7*, 41–58.

(76) Dominguez, N.; Estevez-Herrera, J.; Borges, R.; et al. The Interaction between Chromogranin A and Catecholamines Governs Exocytosis. *FASEB J.* **2014**, *28*, 4657–4667.

(77) He, X.; Ewing, A. G. Simultaneous Counting of Molecules in the Halo and Dense-Core of Nanovesicles by Regulating Dynamics of Vesicle Opening. *Angew. Chem. Int. Ed. Engl.* **2022**, *61*, e202116217.

(78) Rabasco, S.; Nguyen, T. D. K.; Gu, C.; et al. Localization and Absolute Quantification of Dopamine in Discrete Intravesicular Compartments Using NanoSIMS Imaging. *Int. J. Mol. Sci.* **2022**, *23*, 160.

(79) Dunevall, J.; Fathali, H.; Najafinobar, N.; et al. Characterizing the Catecholamine Content of Single Mammalian Vesicles by Collision–Adsorption Events at an Electrode. *J. Am. Chem. Soc.* **2015**, *137*, 4344–4346.

(80) Winkler, H.; Westhead, E. The Molecular Organization of Adrenal Chromaffin Granules. *Neuroscience* **1980**, *5*, 1803–1823.

(81) Santodomingo, J.; Vay, L.; Camacho, M.; et al. Calcium Dynamics in Bovine Adrenal Medulla Chromaffin Cell Secretory Granules. *Eur. J. Neurosci.* **2008**, *28*, 1265–1274.

(82) Videen, J. S.; Mezger, M. S.; Chang, Y. M.; et al. Calcium and Catecholamine Interactions with Adrenal Chromogranins. Comparison of Driving Forces in Binding and Aggregation. *J. Biol. Chem.* **1992**, *267*, 3066–3073.

(83) Yoo, S. H.; Albanesi, J. P.; Jameson, D. M. Fluorescence Studies of Nucleotide Interactions with Bovine Adrenal Chromogranin A. *Biochim. Biophys. Acta* **1990**, *1040*, 66–70.

(84) Kopell, W. N.; Westhead, E. W. Osmotic Pressures of Solutions of ATP and Catecholamines Relating to Storage in Chromaffin Granules. *J. Biol. Chem.* **1982**, *257*, 5707–5710.

(85) Helle, K. B.; Reed, R. K.; Pihl, K. E.; et al. Osmotic Properties of the Chromogranins and Relation to Osmotic Pressure in Catecholamine Storage Granules. *Acta Physiol. Scand.* **1985**, *123*, 21–33.

(86) Camacho, M.; Machado, J. D.; Alvarez, J.; et al. Intravesicular Calcium Release Mediates the Motion and Exocytosis of Secretory Organelles: A Study with Adrenal Chromaffin Cells. *J. Biol. Chem.* **2008**, *283*, 22383–22389.
(87) Mundorf, M. L.; Troyer, K. P.; Hochstetler, S. E.; et al. Vesicular Ca2+ Participates in the Catalysis of Exocytosis. *J. Biol. Chem.* **2000**, *275*, 9136–9142.
(88) Forgac, M. Vacuolar ATPases: Rotary Proton Pumps in Physiology and Pathophysiology. *Nat. Rev. Mol. Cell Biol.* **2007**, *8*, 917–929.
(89) Taupenot, L.; Harper, K. L.; O'Connor, D. T. Role of H+-ATPase-Mediated Acidification in Sorting and Release of the Regulated Secretory Protein Chromogranin A: Evidence for a Vesiculogenic Function. *J. Biol. Chem.* **2005**, *280*, 3885–3897.
(90) Wimalasena, K. Vesicular Monoamine Transporters: Structure-Function, Pharmacology, and Medicinal Chemistry. *Med. Res. Rev.* **2011**, *31*, 483–519.
(91) Moriyama, Y.; Hiasa, M.; Sakamoto, S.; et al. Vesicular Nucleotide Transporter (VNUT): Appearance of an Actress on the Stage of Purinergic Signaling. *Purinergic Signal.* **2017**, *13*, 387–404.
(92) Brady, S. T. Molecular Motors in the Nervous System. *Neuron* **1991**, *7*, 521–533.
(93) Sweeney, H. L.; Holzbaur, E. L. F. Motor Proteins. *Cold Spring Harb. Perspect. Biol.* **2018**, *10*.
(94) Bi, G. Q.; Morris, R. L.; Liao, G.; et al. Kinesin- and Myosin-Driven Steps of Vesicle Recruitment for Ca2+-Regulated Exocytosis. *J. Cell Biol.* **1997**, *138*, 999–1008.
(95) Doreian, B. W.; Fulop, T. G.; Smith, C. B. Myosin II Activation and Actin Reorganization Regulate the Mode of Quantal Exocytosis in Mouse Adrenal Chromaffin Cells. *J. Neurosci. Off. J. Soc. Neurosci.* **2008**, *28*, 4470–4478.
(96) Trouillon, R.; Ewing, A. G. Actin Controls the Vesicular Fraction of Dopamine Released During Extended Kiss and Run Exocytosis. *ACS Chem. Biol.* **2014**, *9*, 812–820.
(97) Lang, T.; Wacker, I.; Wunderlich, I.; et al. Role of Actin Cortex in the Subplasmalemmal Transport of Secretory Granules in PC-12 Cells. *Biophys. J.* **2000**, *78*, 2863–2877.
(98) Felmy, F. Modulation of Cargo Release from Dense Core Granules by Size and Actin Network. *Traffic* **2007**, *8*, 983–997.
(99) Jahn, R.; Fasshauer, D. Molecular Machines Governing Exocytosis of Synaptic Vesicles. *Nature* **2012**, *490*, 201–207.
(100) Südhof, T. C. Neurotransmitter Release: The Last Millisecond in the Life of a Synaptic Vesicle. *Neuron* **2013**, *80*, 675–690.
(101) Verhage, M.; Sørensen, J. B. Vesicle Docking in Regulated Exocytosis. *Traffic* **2008**, *9*, 1414–1424.
(102) Klenchin, V. A.; Martin, T. F. Priming in Exocytosis: Attaining Fusion-Competence after Vesicle Docking. *Biochimie* **2000**, *82*, 399–407.
(103) Südhof, T. C.; Rothman, J. E. Membrane Fusion: Grappling with SNARE and SM Proteins. *Science* **2009**, *323*, 474–477.
(104) Sutton, R. B.; Fasshauer, D.; Jahn, R.; et al. Crystal Structure of a SNARE Complex Involved in Synaptic Exocytosis at 2.4 A Resolution. *Nature* **1998**, *395*, 347–353.
(105) Burkhardt, P.; Hattendorf, D. A.; Weis, W. I.; et al. Munc18a Controls SNARE Assembly through Its Interaction with the Syntaxin N-Peptide. *EMBO J.* **2008**, *27*, 923–933.
(106) Maximov, A.; Tang, J.; Yang, X.; et al. Complexin Controls the Force Transfer from SNARE Complexes to Membranes in Fusion. *Science* **2009**, *323*, 516–521.
(107) Reim, K.; Mansour, M.; Varoqueaux, F.; et al. Complexins Regulate a Late Step in Ca^{2+}-Dependent Neurotransmitter Release. *Cell* **2001**, *104*, 71–81.
(108) Martens, S.; Kozlov, M. M.; McMahon, H. T. How Synaptotagmin Promotes Membrane Fusion. *Science (80-.).* **2007**, *316*, 1205–1208.

(109) Lynch, K. L.; Gerona, R. R. L.; Kielar, D. M.; et al. Synaptotagmin-1 Utilizes Membrane Bending and SNARE Binding to Drive Fusion Pore Expansion. *Mol. Biol. Cell* **2008**, *19*, 5093–5103.
(110) Anantharam, A.; Axelrod, D.; Holz, R. W. Real-Time Imaging of Plasma Membrane Deformations Reveals Pre-Fusion Membrane Curvature Changes and a Role for Dynamin in the Regulation of Fusion Pore Expansion. *J. Neurochem.* **2012**, *122*, 661.
(111) Wu, Q.; Zhang, Q.; Liu, B.; et al. Dynamin 1 Restrains Vesicular Release to a Subquantal Mode In Mammalian Adrenal Chromaffin Cells. *J. Neurosci.* **2019**, *39*, 199 LP – 211.
(112) Amatore, C.; Arbault, S.; Bouret, Y.; et al. Regulation of Exocytosis in Chromaffin Cells by Trans-Insertion of Lysophosphatidylcholine and Arachidonic Acid into the Outer Leaflet of the Cell Membrane. *ChemBioChem* **2006**, *7*, 1998.
(113) Aref, M.; Ranjbari, E.; Romiani, A.; et al. Intracellular Injection of Phospholipids Directly Alters Exocytosis and the Fraction of Chemical Release in Chromaffin Cells as Measured by Nano-Electrochemistry. *Chem. Sci.* **2020**, *11*, 11869–11876.
(114) Lanekoff, I.; Sjövall, P.; Ewing, A. G. Relative Quantification of Phospholipid Accumulation in the PC12 Cell Plasma Membrane Following Phospholipid Incubation Using TOF-SIMS Imaging. *Anal. Chem.* **2011**, *83*, 5337–5343.
(115) Darios, F.; Connell, E.; Davletov, B. Phospholipases and Fatty Acid Signalling in Exocytosis. *J. Physiol.* **2007**, *585*, 699–704.
(116) May, A. P.; Whiteheart, S. W.; Weis, W. I. Unraveling the Mechanism of the Vesicle Transport ATPase NSF, the N-Ethylmaleimide-Sensitive Factor. *J. Biol. Chem.* **2001**, *276*, 21991–21994.
(117) Fatt, P.; Katz, B. Spontaneous Subthreshold Activity at Motor Nerve Endings. *J. Physiol.* **1952**, *117*, 109.
(118) Del Castillo, J Katz, B. Quantal Components of the End-Plate Potential. *J. Physiol.* **1954**, *124*, 560–573.
(119) Ceccarelli, B.; Hurlbut, W. P.; Mauro, A. Turnover of Transmitter and Synaptic Vesicles at the Frog Neuromuscular Junction. *J. Cell Biol.* **1973**, *57*, 499–524.
(120) Fesce, R.; Grohovaz, F.; Valtorta, F.; et al. Neurotransmitter Release: Fusion or "Kiss-and-Run"? *Trends Cell Biol.* **1994**, *4*, 1.
(121) Harata, N. C.; Aravanis, A. M.; Tsien, R. W. Kiss-and-Run and Full-Collapse Fusion as Modes of Exo-Endocytosis in Neurosecretion. *J. Neurochem.* **2006**, *97*, 1546.
(122) He, L.; Wu, L. G. The Debate on the Kiss-and-Run Fusion at Synapses. *Trends Neurosci.* **2007**, *30*, 447–455.
(123) Stevens, C. F.; Williams, J. H. "Kiss and Run" Exocytosis at Hippocampal Synapses. *Proc. Natl. Acad. Sci.* **2000**, *97*, 12828–12833.
(124) Ren, L.; Mellander, L. J.; Keighron, J.; et al. The Evidence for Open and Closed Exocytosis as the Primary Release Mechanism. *Q. Rev. Biophys.* **2016**, *49*, e12.
(125) Obermüller, S.; Lindqvist, A.; Karanauskaite, J.; et al. Selective Nucleotide-Release from Dense-Core Granules in Insulin-Secreting Cells. *J. Cell Sci.* **2005**, *118*, 4271–4282.
(126) Oleinick, A.; Hu, R.; Ren, B.; et al. Theoretical Model of Neurotransmitter Release during In Vivo Vesicular Exocytosis Based on a Grainy Biphasic Nano-Structuration of Chromogranins within Dense Core Matrixes. *J. Electrochem. Soc.* **2015**, *163*, 3014–3024.
(127) Larsson, A.; Majdi, S.; Oleinick, A.; et al. Intracellular Electrochemical Nanomeasurements Reveal That Exocytosis of Molecules at Living Neurons Is Subquantal and Complex. *Angew. Chemie Int. Ed.* **2020**, *59*, 6711–6714.
(128) Phan, N. T. N.; Li, X.; Ewing, A. G. Measuring Synaptic Vesicles Using Cellular Electrochemistry and Nanoscale Molecular Imaging. *Nat. Rev. Chem.* **2017**, *1*, 48.
(129) Wang, Y.; Ewing, A. G. Electrochemical Quantification of Neurotransmitters in Single

Live Cell Vesicles Shows Exocytosis Is Predominantly Partial. *ChemBioChem* **2020**, *22*, 807–813.

(130) Li, X.; Majdi, S.; Dunevall, J.; et al. Quantitative Measurement of Transmitters in Individual Vesicles in the Cytoplasm of Single Cells with Nanotip Electrodes. *Angew. Chem. Int. Ed. Engl.* **2015**, *54*, 11978–11982.

(131) Li, X.; Dunevall, J.; Ewing, A. G. Quantitative Chemical Measurements of Vesicular Transmitters with Electrochemical Cytometry. *Acc. Chem. Res.* **2016**, *49*, 2347–2354.

(132) Wightman, R. M.; Jankowski, J. A.; Kennedy, R. T.; et al. Temporally Resolved Catecholamine Spikes Correspond to Single Vesicle Release from Individual Chromaffin Cells. *Proc. Natl. Acad. Sci. U.S.A.* **1991**, *88*, 10754.

(133) Chen, T. K.; Luo, G.; Ewing, A. G. Amperometric Monitoring of Stimulated Catecholamine Release from Rat Pheochromocytoma (PC12) Cells at the Zeptomole Level. *Anal. Chem.* **1994**, *66*, 3031–3035.

(134) Gu, C.; Larsson, A.; Ewing, A. G. Plasticity in Exocytosis Revealed through the Effects of Repetitive Stimuli Affect the Content of Nanometer Vesicles and the Fraction of Transmitter Released. *Proc. Natl. Acad. Sci.* **2019**, *116*, 21409–21415.

(135) Majdi, S.; Larsson, A.; Najafinobar, N.; et al. Extracellular ATP Regulates the Vesicular Pore Opening in Chromaffin Cells and Increases the Fraction Released During Individual Exocytosis Events. *ACS Chem. Neurosci.* **2019**, *10*, 2459–2466.

(136) Wang, Y.; Gu, C.; Patel, B. A.; et al. Nano-analysis Reveals High Fraction of Serotonin Release during Exocytosis from a Gut Epithelium Model Cell. *Angew. Chemie* **2021**, *60*, 23552–23556.

(137) Hatamie, A.; Ren, L.; Dou, H.; et al. Nanoscale Amperometry Reveals That Only a Fraction of Vesicular Serotonin Content Is Released During Exocytosis from Beta Cells. *Angew. Chem. Int. Ed. Engl.* **2021**, *60*, 7593–7596.

(138) Nguyen, T. D. K.; Rabasco, S.; Lork, A. A.; et al. Quantitative Nanoscale Secondary Ion Mass Spectrometry (NanoSIMS) Imaging of Individual Vesicles to Investigate the Relation between Fraction of Chemical Release and Vesicle Size. *Angew. Chemie Int. Ed.* **2023**, *62*, e202304098.

(139) Cans, A. S.; Hook, F.; Shupliakov, O.; et al. Measurement of the Dynamics of Exocytosis and Vesicle Retrieval at Cell Populations Using a Quartz Crystal Microbalance. *Anal. Chem.* **2001**, *73*, 5805.

(140) Truckenbrodt, S.; Viplav, A.; Jähne, S.; et al. Newly Produced Synaptic Vesicle Proteins Are Preferentially Used in Synaptic Transmission. *EMBO J.* **2018**, *37*, e98044.

(141) Amatore, C.; Oleinick, A. I.; Svir, I. Reconstruction of Aperture Functions during Full Fusion in Vesicular Exocytosis of Neurotransmitters. *ChempPhysChem* **2010**, *11*, 159.

(142) Shin, W.; Arpino, G.; Thiyagarajan, S.; et al. Vesicle Shrinking and Enlargement Play Opposing Roles in the Release of Exocytotic Contents. *Cell Rep.* **2020**, *30*, 421–431.

(143) Nguyen, T. D. K.; Mellander, L.; Lork, A.; et al. Visualization of Partial Exocytotic Content Release and Chemical Transport into Nanovesicles in Cells. *ACS Nano* **2022**, *16*, 4831–4842.

(144) Wierda, K. D. B.; Toonen, R. F. G.; de Wit, H.; et al. Interdependence of PKC-Dependent and PKC-Independent Pathways for Presynaptic Plasticity. *Neuron* **2007**, *54*, 275–290.

(145) Voets, T.; Toonen, R. F.; Brian, E. C.; et al. Munc18-1 Promotes Large Dense-Core Vesicle Docking. *Neuron* **2001**, *31*, 581–591.

(146) Ñeco, P.; Giner, D.; Viniegra, S.; et al. New Roles of Myosin II during Vesicle Transport and Fusion in Chromaffin Cells. *J. Biol. Chem.* **2004**, *279*, 27450–27457.

(147) Elhamdani, A.; Palfrey, H. C.; Artalejo, C. R. Quantal Size Is Dependent on Stimulation Frequency and Calcium Entry in Calf Chromaffin Cells. *Neuron* **2001**, *31*, 819.

(148) Fulop, T.; Smith, C. Matching Native Electrical Stimulation by Graded Chemical Stimulation in Isolated Mouse Adrenal Chromaffin Cells. *J. Neurosci. Methods* **2007**,

166, 195–202.
(149) Ogata, T.; Ogata, A. Henle's Reaction of the Chromaffin Cells in the Adrenals, and the Microscopic Test for Adrenalin. *J. Exp. Med.* **1917**, *25*, 807–817.
(150) Coupland, R. E. The Natural History of the Chromaffin Cell Twenty-Five Years on the Beginning. *Arch. Histol. Cytol.* **1989**, *52*, 331–341.
(151) von Rüden, L.; García, A. G.; López, M. G. The Mechanism of Ba2+-induced Exocytosis from Single Chromaffin Cells. *FEBS Lett.* **1993**, *336*, 48–52.
(152) Heldman, E.; Levine, M.; Raveh, L.; et al. Barium Ions Enter Chromaffin Cells via Voltage-Dependent Calcium Channels and Induce Secretion by a Mechanism Independent of Calcium. *J. Biol. Chem.* **1989**, *264*, 7914–7920.
(153) Tomsig, J. L.; Suszkiw, J. B. Metal Selectivity of Exocytosis in Alpha-Toxin-Permeabilized Bovine Chromaffin Cells. *J. Neurochem.* **1996**, *66*, 644–650.
(154) Blaschko, H.; Welch, A. D. Localization of Adrenaline in Cytoplasmic Particles of the Bovine Adrenal Medulla. *Naunyn. Schmiedebergs. Arch. Exp. Pathol. Pharmakol.* **1953**, *219*, 17–22.
(155) Hillarp, N.-Å.; Lagerstedt, S.; Nilson, B. The Isolation of n Granular Fraction from the Suprarenal Medulla, Containing the Symyathomimetic Catechol Amines1. *Acta Physiol. Scand.* **1953**, *29*, 251–263.
(156) Winkler, H.; Apps, D. K.; Fischer-Colbrie, R. The Molecular Function of Adrenal Chromaffin Granules: Established Facts and Unresolved Topics. *Neuroscience* **1986**, *18*, 261–290.
(157) Albillos, A.; Dernick, G.; Horstmann, H.; et al. The Exocytotic Event in Chromaffin Cells Revealed by Patch Amperometry. *Nature* **1997**, *389*, 509.
(158) Lovrić, J.; Malmberg, P.; Johansson, B. R.; et al. Multimodal Imaging of Chemically Fixed Cells in Preparation for NanoSIMS. *Anal. Chem.* **2016**, *88*, 8841–8848.
(159) Westerink, R. H. S.; Ewing, A. G. The PC12 Cell as Model for Neurosecretion. *Acta Physiol.* **2008**, *192*, 273.
(160) Greene, L. A.; Tischler, A. S. Establishment of a Noradrenergic Clonal Line of Rat Adrenal Pheochromocytoma Cells Which Respond to Nerve Growth Factor. *Proc. Natl. Acad. Sci. U. S. A.* **1976**, *73*, 2424–2428.
(161) Mingorance-Le Meur, A.; Mohebiany, A. N.; O'Connor, T. P. Varicones and Growth Cones: Two Neurite Terminals in PC12 Cells. *PLoS One* **2009**, *4*, e4334.
(162) Coupland, R. E. Electron Microscopic Observations on the Structure of the Rat Adrenal Medulla. *J. Anat.* **1965**, *99*, 231–254.
(163) Colliver, T. L.; Pyott, S. J.; Achalabun, M.; et al. VMAT-Mediated Changes in Quantal Size and Vesicular Volume. *J. Neurosci.* **2000**, *20*, 5276.
(164) Zerby, S. E.; Ewing, A. G. The Latency of Exocytosis Varies with the Mechanism of Stimulated Release in PC12 Cells. *J. Neurochem.* **1996**, *66*, 651–657.
(165) Vaysse, P.-M.; Heeren, R. M. A.; Porta, T.; et al. Mass Spectrometry Imaging for Clinical Research – Latest Developments, Applications, and Current Limitations. *Analyst* **2017**, *142*, 2690–2712.
(166) Wang, T.; Cheng, X.; Xu, H.; et al. Perspective on Advances in Laser-Based High-Resolution Mass Spectrometry Imaging. *Anal. Chem.* **2020**, *92*, 543–553.
(167) Castain, R.; Slodzian, G. Optique Corpusculaire—Premiers Essais de Microanalyse Par Emission Ionique Secondaire. *Comptes Rendus Hebd. Des Seances L Acad. Des Sci.* **1962**, *255*, 1893–1895.
(168) Liebl, H. Ion Microprobe Mass Analyzer. *J. Appl. Phys.* **2004**, *38*, 5277–5283.
(169) Liebl, H. J.; Herzog, R. F. K. Sputtering Ion Source for Solids. *J. Appl. Phys.* **1963**, *34*, 2893–2896.
(170) Benninghoven, A.; Sichtermann, W. K. Detection, Identification, and Structural Investigation of Biologically Important Compounds by Secondary Ion Mass Spectrometry. *Anal. Chem.* **1978**, *50*, 1180–1184.

(171) Slodzian, G.; Hennequin, J. F. Sur Lemission Ionique Secondaire Des Metaux En Presence Doxygene. *Comptes rendus Hebd. des seances l Acad. des Sci. Ser. B* **1966**, *263*, 1246.
(172) Benninghoven, A. Die Positive Sekundärionenemission von Sauerstoffbedeckten Metallen. *Zeitschrift für Naturforsch. A* **1967**, *22*, 841–843.
(173) Storms, H. A.; Brown, K. F.; Stein, J. D. Evaluation of a Cesium Positive Ion Source for Secondary Ion Mass Spectrometry. *Anal. Chem.* **1977**, *49*, 2023–2030.
(174) Winograd, N. The Magic of Cluster SIMS. *Anal. Chem.* **2005**, *77*, 142–149.
(175) CAMECA. NanoSIMS 50L - SIMS Microprobe for Isotopic and Trace Element Analysis at High Spatial Resolution https://www.cameca.com/products/sims/nanosims (accessed Oct 22, 2023).
(176) Meibom, A.; Plane, F.; Cheng, T.; et al. Correlated Cryo-SEM and CryoNanoSIMS Imaging of Biological Tissue. *BMC Biol.* **2023**, *21*, 126.
(177) Ionoptika. IOG 25GA. 25 kV Focused Ion Beam https://ionoptika.com/products/ion-beams/liquid-metal-ion-beams/iog-25ga/ (accessed Oct 22, 2023).
(178) Nuñez, J.; Renslow, R.; Cliff, J. B.; et al. NanoSIMS for Biological Applications: Current Practices and Analyses. *Biointerphases* **2017**, *13*, 03B301.
(179) Siuzdak, G. Subcellular Quantitative Imaging of Metabolites at the Organelle Level. *Nat. Metab.* **2023**, *5*, 1446–1448.
(180) Caprioli, R. M.; Farmer, T. B.; Gile, J. Molecular Imaging of Biological Samples: Localization of Peptides and Proteins Using MALDI-TOF MS. *Anal. Chem.* **1997**, *69*, 4751–4760.
(181) Spengler, B.; Hubert, M.; Kaufmann, R. MALDI Ion Imaging and Biological Ion Imaging with a New Scanning UV-Laser Microprobe. In *Proceedings of the 42nd Annual Conference on Mass Spectrometry and Allied Topics*; Chicago Illinois, 1994; Vol. 1041, p. 1041.
(182) Tanaka, K.; Waki, H.; Ido, Y.; et al. Protein and Polymer Analyses up to m/z 100 000 by Laser Ionization Time-of-flight Mass Spectrometry. *Rapid Commun. mass Spectrom.* **1988**, *2*, 151–153.
(183) Cornett, D. S.; Frappier, S. L.; Caprioli, R. M. MALDI-FTICR Imaging Mass Spectrometry of Drugs and Metabolites in Tissue. *Anal. Chem.* **2008**, *80*, 5648–5653.
(184) Moreno-Gordaliza, E.; Esteban-Fernández, D.; Lázaro, A.; et al. MALDI-LTQ-Orbitrap Mass Spectrometry Imaging for Lipidomic Analysis in Kidney under Cisplatin Chemotherapy. *Talanta* **2017**, *164*, 16–26.
(185) Wang, X.; Han, J.; Chou, A.; et al. Hydroxyflavones as a New Family of Matrices for MALDI Tissue Imaging. *Anal. Chem.* **2013**, *85*, 7566–7573.
(186) Wang, X.; Han, J.; Pan, J.; et al. Comprehensive Imaging of Porcine Adrenal Gland Lipids by MALDI-FTMS Using Quercetin as a Matrix. *Anal. Chem.* **2014**, *86*, 638–646.
(187) Esteve, C.; Tolner, E. A.; Shyti, R.; et al. Mass Spectrometry Imaging of Amino Neurotransmitters: A Comparison of Derivatization Methods and Application in Mouse Brain Tissue. *Metabolomics* **2016**, *12*, 30.
(188) Holst, S.; Heijs, B.; De Haan, N.; et al. Linkage-Specific in Situ Sialic Acid Derivatization for N-Glycan Mass Spectrometry Imaging of Formalin-Fixed Paraffin-Embedded Tissues. *Anal. Chem.* **2016**, *88*, 5904–5913.
(189) Takáts, Z.; Wiseman, J. M.; Gologan, B.; et al. Mass Spectrometry Sampling under Ambient Conditions with Desorption Electrospray Ionization. *Science* **2004**, *306*, 471–473.
(190) Kertesz, V.; Van Berkel, G. J. Improved Imaging Resolution in Desorption Electrospray Ionization Mass Spectrometry. *Rapid Commun. Mass Spectrom.* **2008**, *22*, 2639–2644.
(191) Laskin, J.; Heath, B. S.; Roach, P. J.; et al. Tissue Imaging Using Nanospray Desorption

Electrospray Ionization Mass Spectrometry. *Anal. Chem.* **2012**, *84*, 141–148.
(192) Passarelli, M. K.; Ewing, A. G. Single-Cell Imaging Mass Spectrometry. *Curr. Opin. Chem. Biol.* **2013**, *17*, 854–859.
(193) Hanrieder, J.; Phan, N. T. N.; Kurczy, M. E.; et al. Imaging Mass Spectrometry in Neuroscience. *ACS Chem. Neurosci.* **2013**, *4*, 666–679.
(194) Hanrieder, J.; Ljungdahl, A.; Fälth, M.; et al. L-DOPA-Induced Dyskinesia Is Associated with Regional Increase of Striatal Dynorphin Peptides as Elucidated by Imaging Mass Spectrometry. *Mol. Cell. Proteomics* **2011**, *10*, M111.009308.
(195) Solé-Domènech, S.; Sjövall, P.; Vukojević, V.; et al. Localization of Cholesterol, Amyloid and Glia in Alzheimer's Disease Transgenic Mouse Brain Tissue Using Time-of-Flight Secondary Ion Mass Spectrometry (ToF-SIMS) and Immunofluorescence Imaging. *Acta Neuropathol.* **2013**, *125*, 145–157.
(196) Carreira, R. J.; Shyti, R.; Balluff, B.; et al. Large-Scale Mass Spectrometry Imaging Investigation of Consequences of Cortical Spreading Depression in a Transgenic Mouse Model of Migraine. *J. Am. Soc. Mass Spectrom.* **2015**, *26*, 853–861.
(197) Stoeckli, M.; Staab, D.; Staufenbiel, M.; et al. Molecular Imaging of Amyloid Beta Peptides in Mouse Brain Sections Using Mass Spectrometry. *Anal. Biochem.* **2002**, *311*, 33–39.
(198) Shariatgorji, M.; Nilsson, A.; Fridjonsdottir, E.; et al. Comprehensive Mapping of Neurotransmitter Networks by MALDI–MS Imaging. *Nat. Methods* **2019**, *16*, 1021–1028.
(199) Passarelli, M. K.; Pirkl, A.; Moellers, R.; et al. The 3D OrbiSIMS - Label-Free Metabolic Imaging with Subcellular Lateral Resolution and High Mass-Resolving Power. *Nat. Methods* **2017**, *14*, 1175–1183.
(200) Shariatgorji, M.; Nilsson, A.; Goodwin, R. J. A.; et al. Direct Targeted Quantitative Molecular Imaging of Neurotransmitters in Brain Tissue Sections. *Neuron* **2014**, *84*, 697–707.
(201) Kaya, I.; Brülls, S. M.; Dunevall, J.; et al. On-Tissue Chemical Derivatization of Catecholamines Using 4- (N-Methyl) Pyridinium Boronic Acid for ToF-SIMS and LDI-ToF Mass Spectrometry Imaging. *Anal. Chem.* **2018**, *90*, 13580–13590.
(202) Sugiura, Y.; Zaima, N.; Setou, M.; et al. Visualization of Acetylcholine Distribution in Central Nervous System Tissue Sections by Tandem Imaging Mass Spectrometry. *Anal. Bioanal. Chem.* **2012**, *403*, 1851–1861.
(203) Vallianatou, T.; Shariatgorji, M.; Nilsson, A.; et al. Molecular Imaging Identifies Age-Related Attenuation of Acetylcholine in Retrosplenial Cortex in Response to Acetylcholinesterase Inhibition. *Neuropsychopharmacol. Off. Publ. Am. Coll. Neuropsychopharmacol.* **2019**, *44*, 2091–2098.
(204) Lovrić, J.; Dunevall, J.; Larsson, A.; et al. Nano Secondary Ion Mass Spectrometry Imaging of Dopamine Distribution Across Nanometer Vesicles. *ACS Nano* **2017**, *11*, 3446–3455.
(205) Thomen, A.; Najafinobar, N.; Penen, F.; et al. Sub-Cellular Mass Spectrometry Imaging and Absolute Quantitative Analysis across Organelles. *ACS Nano* **2020**, *14*, 4316–4325.
(206) Wu, C.; Ifa, D. R.; Manicke, N. E.; et al. Molecular Imaging of Adrenal Gland by Desorption Electrospray Ionization Mass Spectrometry. *Analyst* **2010**, *135*, 28–32.
(207) Maciel, L. I. L.; Pereira, I.; Ramalho, R. R. F.; et al. A New Approach for the Analysis of Amino Acid Neurotransmitters in Mouse Brain Tissues Using DESI Imaging. *Int. J. Mass Spectrom.* **2022**, *471*, 116730.
(208) Pace, C. L.; Horman, B.; Patisaul, H.; et al. Analysis of Neurotransmitters in Rat Placenta Exposed to Flame Retardants Using IR-MALDESI Mass Spectrometry Imaging. *Anal. Bioanal. Chem.* **2020**, *412*, 3745–3752.
(209) Bagley, M. C.; Ekelöf, M.; Rock, K.; et al. IR-MALDESI Mass Spectrometry Imaging

of Underivatized Neurotransmitters in Brain Tissue of Rats Exposed to Tetrabromobisphenol A. *Anal. Bioanal. Chem.* **2018**, *410*, 7979–7986.

(210) Manier, M. L.; Spraggins, J. M.; Reyzer, M. L.; et al. A Derivatization and Validation Strategy for Determining the Spatial Localization of Endogenous Amine Metabolites in Tissues Using MALDI Imaging Mass Spectrometry. *J. Mass Spectrom.* **2014**, *49*, 665–673.

(211) Chen, C.; Laviolette, S. R.; Whitehead, S. N.; et al. Imaging of Neurotransmitters and Small Molecules in Brain Tissues Using Laser Desorption/Ionization Mass Spectrometry Assisted with Zinc Oxide Nanoparticles. *J. Am. Soc. Mass Spectrom.* **2021**, *32*, 1065–1079.

(212) Ito, T.; Hiramoto, M. Use of MTRAQ Derivatization Reagents on Tissues for Imaging Neurotransmitters by MALDI Imaging Mass Spectrometry: The Triple Spray Method. *Anal. Bioanal. Chem.* **2019**, *411*, 6847–6856.

(213) Sugiyama, E.; Guerrini, M. M.; Honda, K.; et al. Detection of a High-Turnover Serotonin Circuit in the Mouse Brain Using Mass Spectrometry Imaging. *iScience* **2019**, *20*, 359–372.

(214) Zhang, D.-S.; Piazza, V.; Perrin, B. J.; et al. Multi-Isotope Imaging Mass Spectrometry Reveals Slow Protein Turnover in Hair-Cell Stereocilia. *Nature* **2012**, *481*, 520–524.

(215) Frisz, J. F.; Lou, K.; Klitzing, H. A.; et al. Direct Chemical Evidence for Sphingolipid Domains in the Plasma Membranes of Fibroblasts. *Proc. Natl. Acad. Sci.* **2013**, *110*, 613–622.

(216) Steinhauser, M. L.; Bailey, A. P.; Senyo, S. E.; et al. Multi-Isotope Imaging Mass Spectrometry Quantifies Stem Cell Division and Metabolism. *Nature* **2012**, *481*, 516–519.

(217) Rabasco, S.; Lork, A. A.; Berlin, E.; et al. Characterization of Stress Granule Protein Turnover in Neuronal Progenitor Cells Using Correlative STED and NanoSIMS Imaging. *International Journal of Molecular Sciences*, 2023, *24*.

(218) Kabatas, S.; Agüi-Gonzalez, P.; Saal, K.-A.; et al. Boron-Containing Probes for Non-Optical High-Resolution Imaging of Biological Samples. *Angew. Chemie Int. Ed.* **2019**, *58*, 3438–3443.

(219) Kabatas, S.; Agüi-Gonzalez, P.; Hinrichs, R.; et al. Fluorinated Nanobodies for Targeted Molecular Imaging of Biological Samples Using Nanoscale Secondary Ion Mass Spectrometry. *J. Anal. At. Spectrom.* **2019**, *34*, 1083–1087.

(220) Lee, R. F. S.; Riedel, T.; Escrig, S.; et al. Differences in Cisplatin Distribution in Sensitive and Resistant Ovarian Cancer Cells: A TEM/NanoSIMS Study. *Metallomics* **2017**, *9*, 1413–1420.

(221) Jiang, H.; Passarelli, M. K.; Munro, P. M. G.; et al. High-Resolution Sub-Cellular Imaging by Correlative NanoSIMS and Electron Microscopy of Amiodarone Internalisation by Lung Macrophages as Evidence for Drug-Induced Phospholipidosis. *Chem. Commun.* **2017**, *53*, 1506–1509.

(222) Becquart, C.; Stulz, R.; Thomen, A.; et al. Intracellular Absolute Quantification of Oligonucleotide Therapeutics by NanoSIMS. *Anal. Chem.* **2022**, *94*, 10549–10556.

(223) He, C.; Migawa, M. T.; Chen, K.; et al. High-Resolution Visualization and Quantification of Nucleic Acid–Based Therapeutics in Cells and Tissues Using Nanoscale Secondary Ion Mass Spectrometry (NanoSIMS). *Nucleic Acids Res.* **2021**, *49*, 1–14.

(224) Nuñez, J.; Renslow, R.; Cliff, J. B.; et al. NanoSIMS for Biological Applications: Current Practices and Analyses. *Biointerphases* **2017**, *13*, 03B301.

(225) CAMECA. NanoSIMS 50L Application Booklet - Instrumentation https://www.cameca.com/learning-zone/application-notes/sims (accessed Oct 24, 2023).

(226) Murray, K. K. Resolution and Resolving Power in Mass Spectrometry. *J. Am. Soc.*

Mass Spectrom. **2022**, *33*, 2342–2347.
(227) Laeter, J. R. de; Böhlke, J. K.; Bièvre, P. De; et al. Atomic Weights of the Elements. Review 2000 (IUPAC Technical Report). *Pure Appl. Chem.* **2003**, *75*, 683–800.
(228) Nuñez, J.; Renslow, R.; Cliff, J. B.; et al. NanoSIMS for Biological Applications: Current Practices and Analyses. *Biointerphases* **2018**, *13*, 03B301.
(229) CAMECA. Dynamic Secondary Ion Mass Spectrometry https://www.cameca.com/company/news/2019/august/dynamic-sims-ekb-tutorial (accessed Oct 22, 2023).
(230) De Broglie, L. The Wave Nature of the Electron. *Nobel Lect.* **1929**, *12*, 244–256.
(231) Ruska, E. The Development of the Electron Microscope and of Electron Microscopy. *Rev. Mod. Phys.* **1987**, *59*, 627.
(232) The Nobel Prize in Physics 1986 https://www.nobelprize.org/prizes/physics/1986/summary/ (accessed Oct 29, 2023).
(233) Dubochet, J.; McDowall, A. W. Vitrification of Pure Water for Electron Microscopy. *J. Microsc.* **1981**, *124*, 3–4.
(234) Dubochet, J. Cryo-EM—the First Thirty Years. *J. Microsc.* **2012**, *245*, 221–224.
(235) Fan, X.; Wang, J.; Zhang, X.; et al. Single Particle Cryo-EM Reconstruction of 52 KDa Streptavidin at 3.2 Angstrom Resolution. *Nat. Commun.* **2019**, *10*, 2386.
(236) Bogner, A.; Jouneau, P.-H.; Thollet, G.; et al. A History of Scanning Electron Microscopy Developments: Towards "Wet-STEM" Imaging. *Micron* **2007**, *38*, 390–401.
(237) Eswara, S.; Pshenova, A.; Yedra, L.; et al. Correlative Microscopy Combining Transmission Electron Microscopy and Secondary Ion Mass Spectrometry: A General Review on the State-of-the-Art, Recent Developments, and Prospects. *Appl. Phys. Rev.* **2019**, *6*.
(238) Hoffman, E. A.; Frey, B. L.; Smith, L. M.; et al. Formaldehyde Crosslinking: A Tool for the Study of Chromatin Complexes *. *J. Biol. Chem.* **2015**, *290*, 26404–26411.
(239) Roozemond, R. C. The Effect of Fixation with Formaldehyde and Glutaraldehyde on the Composition of Phospholipids Extractable from Rat Hypothalamus. *J. Histochem. Cytochem.* **1969**, *17*, 482–486.
(240) Morris, J. K. A Formaldehyde Glutaraldehyde Fixative of High Osmolality for Use in Electron Microscopy. *J. cell Biol* **1965**, *27*, 1A-149A.
(241) Sanderson, M. J.; Smith, I.; Parker, I.; et al. Fluorescence Microscopy. *Cold Spring Harb. Protoc.* **2014**, 1042–1065.
(242) Sanderson, M. J.; Smith, I.; Parker, I.; et al. Fluorescence Microscopy. *Cold Spring Harb. Protoc.* **2014**, *2014*, pdb.top071795.
(243) Göttfert, F.; Wurm, C. A.; Mueller, V.; et al. Coaligned Dual-Channel STED Nanoscopy and Molecular Diffusion Analysis at 20 Nm Resolution. *Biophysical journal*, 2013, *105*, L01-3.
(244) Vicidomini, G.; Bianchini, P.; Diaspro, A. STED Super-Resolved Microscopy. *Nat. Methods* **2018**, *15*, 173–182.
(245) Hell, S. W.; Wichmann, J. Breaking the Diffraction Resolution Limit by Stimulated Emission: Stimulated-Emission-Depletion Fluorescence Microscopy. *Opt. Lett.* **1994**, *19*, 780–782.
(246) Schermelleh, L.; Ferrand, A.; Huser, T.; et al. Super-Resolution Microscopy Demystified. *Nat. Cell Biol.* **2019**, *21*, 72–84.
(247) Calovi, S.; Soria, F. N.; Tønnesen, J. Super-Resolution STED Microscopy in Live Brain Tissue. *Neurobiol. Dis.* **2021**, *156*, 105420.
(248) Chalfie, M.; Tu, Y.; Euskirchen, G.; et al. Green Fluorescent Protein as a Marker for Gene Expression. *Science* **1994**, *263*, 802–805.
(249) Prasher, D. C.; Eckenrode, V. K.; Ward, W. W.; et al. Primary Structure of the Aequorea Victoria Green-Fluorescent Protein. *Gene* **1992**, *111*, 229–233.

(250) Proteintech. GFP (green fluorescent protein): Properties, origin, specifications, tips https://www.ptglab.com/news/blog/gfp-green-fluorescent-protein-properties-origin-specifications-tips/ (accessed Nov 2, 2023).
(251) Los, G. V; Encell, L. P.; McDougall, M. G.; et al. HaloTag: A Novel Protein Labeling Technology for Cell Imaging and Protein Analysis. *ACS Chem. Biol.* **2008**, *3*, 373–382.
(252) Proteintech. Halotag https://www.ptglab.com/news/blog/halotag/ (accessed Nov 2, 2023).
(253) Miesenböck, G.; De Angelis, D. A.; Rothman, J. E. Visualizing Secretion and Synaptic Transmission with PH-Sensitive Green Fluorescent Proteins. *Nature* **1998**, *394*, 192–195.
(254) Zhu, D.; Zhou, W.; Liang, T.; et al. Synaptotagmin I and IX Function Redundantly in Controlling Fusion Pore of Large Dense Core Vesicles. *Biochem. Biophys. Res. Commun.* **2007**, *361*, 922.
(255) Hettie, K. S.; Liu, X.; Gillis, K. D.; et al. Fluorescent Sensor for the Visualization of Norepinephrine in Fixed. *ACS Chem. Neurosci.* **2013**, *4*, 914–923.
(256) Gubernator, N. G.; Zhang, H.; Staal, R. G. W. W.; et al. Fluorescent False Neurotransmitters Visualize Dopamine Release from Individual Presynaptic Terminals. *Science.* **2009**, *324*, 1441–1444.
(257) Lee, M.; Gubernator, N. G.; Sulzer, D.; et al. Development of PH-Responsive Fluorescent False Neurotransmitters. *J. Am. Chem. Soc.* **2010**, *132*, 8828–8830.
(258) Dunn, M.; Henke, A.; Clark, S.; et al. Designing a Norepinephrine Optical Tracer for Imaging Individual Noradrenergic Synapses and Their Activity in Vivo. *Nat. Commun.* **2018**, *9*, 1–13.
(259) Shin, W.; Wei, L.; Arpino, G.; et al. Preformed Ω-Profile Closure and Kiss-and-Run Mediate Endocytosis and Diverse Endocytic Modes in Neuroendocrine Chromaffin Cells. *Neuron* **2021**, *109*, 3119-3134.e5.
(260) Amaral, E.; Guatimosim, S.; Guatimosim, C. Using the Fluorescent Styryl Dye FM1-43 to Visualize Synaptic Vesicles Exocytosis and Endocytosis in Motor Nerve Terminals. *Methods Mol. Biol.* **2011**, *689*, 137–148.
(261) Revelo, N. H.; Kamin, D.; Truckenbrodt, S.; et al. A New Probe for Super-Resolution Imaging of Membranes Elucidates Trafficking Pathways. *J. Cell Biol.* **2014**, *205*, 591–606.
(262) Najafinobar, N.; Lovrić, J.; Majdi, S.; et al. Excited Fluorophores Enhance the Opening of Vesicles at Electrode Surfaces in Vesicle Electrochemical Cytometry. *Angew. Chemie Int. Ed.* **2016**, *55*, 15081–15085.
(263) Zheng, Y.-N.; Nguyen, T. D. K.; Dunevall, J.; et al. Dynamic Visualization and Quantification of Single Vesicle Opening and Content by Coupling Vesicle Impact Electrochemical Cytometry with Confocal Microscopy. *ACS Meas. Sci. Au* **2021**, *1*, 131–138.
(264) Meulemans, A.; Poulain, B.; Baux, G.; et al. Changes in Serotonin Concentration in a Living Neurone: A Study by on-Line Intracellular Voltammetry. *Brain Res.* **1987**, *414*, 158–162.
(265) Leszczyszyn, D. J.; Jankowski, J. A.; Viveros, O. H.; et al. Nicotinic Receptor-Mediated Catecholamine Secretion from Individual Chromaffin Cells. Chemical Evidence for Exocytosis. *J. Biol. Chem.* **1990**, *265*, 14736–14737.
(266) Roberts, J. G.; Mitchell, E. C.; Dunaway, L. E.; et al. Carbon-Fiber Nanoelectrodes for Real-Time Discrimination of Vesicle Cargo in the Native Cellular Environment. *ACS Nano* **2020**, *14*, 2917–2926.
(267) Zhou, Z.; Misler, S. Amperometric Detection of Stimulus-Induced Quantal Release of Catecholamines from Cultured Superior Cervical Ganglion Neurons. *Proc. Natl. Acad. Sci. U. S. A.* **1995**, *92*, 6938–6942.
(268) Pothos, E. N.; Davila, V.; Sulzer, D. Presynaptic Recording of Quanta from Midbrain

Dopamine Neurons and Modulation of the Quantal Size. *J. Neurosci.* **1998**, *18*, 4106.
(269) Zhang, Q.; Liu, B.; Wu, Q.; et al. Differential Co-Release of Two Neurotransmitters from a Vesicle Fusion Pore in Mammalian Adrenal Chromaffin Cells. *Neuron* **2019**, *102*, 173-183.e4.
(270) Bruns, D.; Jahn, R. Real-Time Measurement of Transmitter Release from Single Synaptic Vesicles. *Nature* **1995**, *377*, 62–65.
(271) Majdi, S.; Berglund, E. C.; Dunevall, J.; et al. Electrochemical Measurements of Optogenetically Stimulated Quantal Amine Release from Single Nerve Cell Varicosities in Drosophila Larvae. *Angew. Chem. Int. Ed. Engl.* **2015**, *54*, 13609–13612.
(272) Lovrić, J.; Najafinobar, N.; Dunevall, J.; et al. On the Mechanism of Electrochemical Vesicle Cytometry: Chromaffin Cell Vesicles and Liposomes. *Faraday Discuss.* **2016**, *193*, 65–79.
(273) Li, X.; Ewing, A.; Dunevall, J.; et al. Mechanistic Aspects of Vesicle Opening during Analysis with Vesicle Impact Electrochemical Cytometry. *j* **2017**, *89*.
(274) Willig, K. I.; Rizzoli, S. O.; Westphal, V.; et al. STED Microscopy Reveals That Synaptotagmin Remains Clustered after Synaptic Vesicle Exocytosis. *Nature* **2006**, *440*, 935–939.
(275) Midorikawa, M. Real-Time Imaging of Synaptic Vesicle Exocytosis by Total Internal Reflection Fluorescence (TIRF) Microscopy. *Neurosci. Res.* **2018**, *136*, 1–5.